

AMERICAN UNIVERSITY OF BEIRUT

SUPERIOR REMOVAL OF ARSENIC AND LEAD FROM
WATER USING ZINC BASED METAL ORGANIC
FRAMEWORK ZN-MOF-74

by
ALI MOURIES CHOUMAN

A thesis
submitted in partial fulfillment of the requirements
for the degree of Master of Science
to the Department of Chemical and Petroleum Engineering
of the Maroun Semaan Faculty of Engineering and Architecture
at the American University of Beirut

Beirut, Lebanon
June 2018

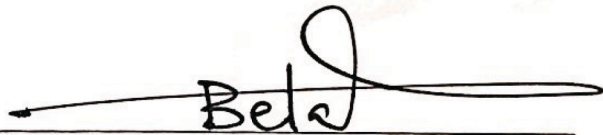
ii

AMERICAN UNIVERSITY OF BEIRUT

SUPERIOR REMOVAL OF ULTRA-TRACE ARSENIC AND LEAD
FROM WATER USING NANO-SIZED ZINC METAL ORGANIC
FRAMEWORK ZN-MOF-74

by
ALI MOURIES CHOUMAN

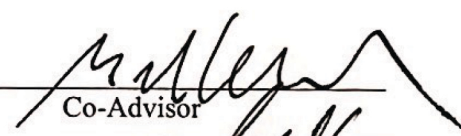
Approved by:



Dr. Belal Abu Tarboush, Assistant Professor
Department of Chemical and Petroleum Engineering

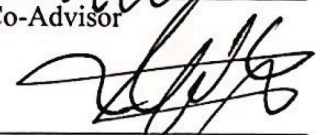
Advisor

Dr. Mazen Al-Ghoul, Professor
Department of Chemistry



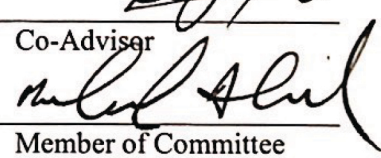
Co-Advisor

Dr. Mohamad Hmadeh, Assistant Professor
Department of Chemistry



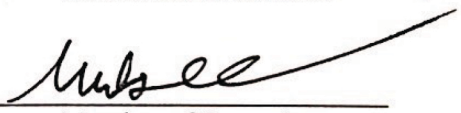
Co-Advisor

Dr. Mohammad N. Ahmad, Professor, Chairman
Department of Chemical and Petroleum Engineering



Member of Committee

Dr. Mutasem Shehadeh, Associate Professor
Department of Mechanical Engineering



Member of Committee

Date of thesis defense: July 5, 2018

ACKNOWLEDGMENTS

I would like to express my deepest gratitude and appreciation to my thesis advisor Dr. Belal Abu Tarboush for his great guidance and assistance throughout my research.

I would like to also thank my thesis Co-Advisors, Dr. Mazen Al-Ghoul and Dr. Mohamad Hmadeh for their valuable advice and encouragement at all stages of this work.

Special thanks to Dr. Mohammad Ahmad and Dr. Mutasem Shehadeh for their constructive comments and suggestions on the manuscript of my thesis paper.

Finally, I would like to thank my dearest family and friends for their great encouragement, support, and unconditional love. Their faith in my capabilities has motivated me to accomplish this work with all confidence and persistence.

AN ABSTRACT OF THE THESIS OF

Ali Mouries Chouman for

Master of Science

Major: Chemical Engineering

Title: Superior Removal of Arsenic and Lead From water Using Zinc Based Metal Organic Framework Zn-MOF-74

This study investigates and compares the removal of As(V) and Pb(II) from aqueous media using the water-stable zinc-metal organic frameworks (Zn-MOF-74) prepared via room-temperature precipitation (RT-Zn-MOF-74) and solvothermal procedure (HT-Zn-MOF-74). The Zn-MOF-74 crystals possess an average particle size of 66 nm and 144 μm for RT-Zn-MOF-74 and HT-Zn-MOF-74, respectively. Moreover, the nano-sized RT-Zn-MOF-74 exhibited superior performance to that of HT-Zn-MOF-74. While the BET surface area of the RT-Zn-MOF-74 was smaller than the HT-Zn-MOF-74, higher adsorption took place onto the room temperature synthesized ones, owing to their small particle size and better dispersion. Adsorption isotherm studies showed that Langmuir isotherm was effective for the adsorption of As(V) onto RT-Zn-MOF-74 and HT-Zn-MOF-74 with a maximum adsorption capacity (q_{max}) value of 99.0 mg g^{-1} and 48.7 mg g^{-1} , respectively. Also Langmuir model was able to describe the data of Pb(II) removal using both RT and HT Zn-MOF-74 with adsorption capacities capacity (q_{max}) value of 487 mg g^{-1} and 329.13 mg g^{-1} respectively. These values exceed most reported maximum adsorption capacities at neutral pH and in the case of Pb(II) removal, 487 mg g^{-1} is the highest ever reported lead adsorption capacity in the literature. The thermodynamics of As(V) adsorption revealed a spontaneous highly endothermic process ($\Delta H=46.2 \text{ KJ mol}^{-1}$) that is due to the substitution of adsorbed water molecules by arsenate in the pores of the MOF crystal resulting in a chemical adsorption process. For the removal of Pb(II) ions, the process was also found to be spontaneous and slightly endothermic ($\Delta H=20.9 \text{ KJ mol}^{-1}$) and the main force controlling the interaction between Pb^{2+} and Zn-MOF-74 is Van der Waals resulting in a physical adsorption process. This was further investigated using plane-wave density functional theory (DFT) calculations. This study constitutes a direct evidence for the importance of tuning the size of MOF crystals to enhance their properties.

CONTENTS

ACKNOWLEDGEMENTS	v
ABSTRACT.....	vi
LIST OF ILLUSTRATIONS.....	xii
LIST OF TABLES.....	xiii
I. INTRODUCTION.....	1
II. LITERATURE REVIEW.....	6
A. Chemical Oxidation	6
B. Chemical Precipitation.....	7
C. Chemical Coagulation	8
D. Chemical Stabilization	9
E. Ion Exchange.....	9
F. Membrane Filtration.....	10
G. Adsorption.....	11
III. METHODOLOGY.....	17
A. Synthesis and Reagents	17
B. Characterization.....	19
C. As(V) Adsorption Experiments.....	20
D. Pb(II) Adsorption Experiments.....	22

III. CHARACTERIZATION OF ZN-MOF-74.....	26
IV. ADSORPTION OF ARSENATE.....	31
A. Effects of pH.....	31
B. Effects of Temperature.....	33
C. Adsorption Kinetics.....	34
D. Adsorption Isotherm.....	38
E. Thermodynamics Analysis.....	43
F. Adsorption Energies via DFT Calculations.....	45
V. ADSORPTION OF LEAD IONS.....	48
A. Effects of pH on Lead Adsorption and Surface Charge.....	48
B. Effects of Adding salts to the adsorbate solution.....	51
C. Effects of Contact Time and Temperature.....	52
D. Effect of Particle Size.....	54
E. Adsorption Isotherm.....	55
F. Adsorption Kinetics.....	58
G. Effect of Adsorbent Dosage.....	62
H. Thermodynamics.....	63
VI. CONCLUSION.....	66

Appendix

I. SAMPLE CALCULATIONS AND SUPPORTING INFO.. 67

BIBLIOGRAPHY74

ILLUSTRATIONS

Figure	Page
1. Crystal Structure of Zn-MOF-74.....	18
2. XRD Analysis of Zn-MOF-74 before and after adsorption of As(V) (A). TGA analysis of Zn-MOF-74 before and after adsorption of As (V) (B). N ₂ Isotherms of RT-Zn-MOF-74 and HT-Zn-MOF-74 (C)...	31
3. SEM images of RT-Zn-MOF-74 and HT-Zn-MOF-74 (A,B,C,D).....	32
4. Effects of contact time on the removal of As(V) by the adsorbent Zn-MOF-74. C ₀ = 40 mg L ⁻¹ , V = 10 mL, m = 10 mg	38
5. Langmuir and Freundlich isotherms for As(V) removal.....	44
6. Effects of the mass of adsorbent on the removal efficiency of As(V)....	45
7. Energy level diagram of the adsorption of water and arsenate on Zn-MOF-74	50
8. Effect of pH on the removal efficiency and surface charge.....	54
9. Effect of adding salts on the removal efficiency of Pb(II).....	57
10. Effect of contact time and temperature on removal of Pb(II)	59
11. Effect of initial sorbent concentration of the adsorption capacity	64
12. Pseudo first and second order kinetics for the removal of Pb(II)	68
13. Langmuir Freundlich and D-R isotherm models for Pb(II) removal.....	68
14. Effect of adsorbent dosage on adsorption capacity.....	70
15. Van't Hof plot of ln(K) versus inverse temperature.....	72
S1. Effects of pH on the percent removal of As(V), by the adsorbent Zn-MOF-74(A). Effects of Temperature on the As(V) removal by the adsorbent Zn-MOF-74(B).	75
S2. FT-IR spectra of RT and HT-Zn-MOF-74 before and after adsorption of As(V).	76
S3. Intraparticle diffusion kinetics of As(V) on RT-Zn-MOF-74 nanoparticles.	77

S4.	Effect of initial concentration of As(V) on the adsorption onto RT-Zn-MOF-74 and HT-Zn-MOF-74.	78
S5.	Van't Hof plot of $\ln(K)$ versus inverse temperature.	79

TABLES

Table		Page
1.	Reported adsorbents used for removing As(V) and Pb(II) from water...	14
2.	Parameters of As(V) adsorption kinetics by Zn-MOF-74.....	36
3.	The Langmuir and Freundlich parameters and correlation coefficients for arsenate adsorption onto RT-Zn-MOF-74 and HT-Zn-MOF-74.....	41
4.	Thermodynamic parameters at T = 20 °C, 30 °C, 35 °C and 40 °C.....	45
5.	The Langmuir, Freundlich, and R-D parameters for Pb (II) adsorption.	55
6.	Parameters of Pb(II) adsorption kinetics by Zn-MOF-74.....	54
7.	Thermodynamic properties at T= 25°C, 30°C, 35°C, 40°C, 50°C.....	66
S1.	Sample calculation for isotherm models parameters in the adsorption of Arsenic As(V).	80
S2.	Sample calculation for isotherm models parameters in the adsorption of lead.	81

CHAPTER I

INTRODUCTION

Heavy metals in water introduce high risks of health and environmental issues, and arsenic is one of these metals causing threat to millions of people[1]. Arsenic is an odorless and tasteless metalloid that can exist in various chemical forms either organic or inorganic[2]. It is the 20th most abundant trace element in the earth's crust, present most often as arsenic sulfide or as metal arsenate and arsenite[3]. It is also present in the air, water, soil and rocks. Nonetheless, its concentration varies depending on the natural conditions or human activities. Arsenic's average concentration in earth is approximately 5 mg/L[4]. The inorganic form of Arsenic is highly toxic, and naturally present as arsenate at high levels in the under-groundwater for various countries including: Argentina, Bangladesh, China, the United States of America[5]. High levels of Inorganic arsenic in water present a great threat to public health. Human beings can be exposed to arsenic through: Drinking-water, smoking tobacco, industrial processes, crops irrigated with contaminated water and food prepared with contaminated water. According to the World Health Organization (WHO) and the Environmental Protection Agency (E.P.A), the threshold concentration of arsenic in the drinking water is 10 $\mu\text{g/L}$ [6, 7].

Arsenic could have acute or long-term lingering effects. For acute arsenic poisoning immediate symptoms like vomiting, abdominal pain and diarrhea are observed[8]. When it goes to extreme exposure, death can occur. Long-term exposure to high levels of inorganic arsenic could lead to adverse effect on human skin ranging from pigmentation changes, to skin lesions and hyperkeratosis[9]. According to The International Agency for Research on Cancer (IARC), arsenic compounds are regarded to be carcinogenic to humans, hence long-term exposure to high levels of inorganic arsenic could cause different types of cancers, particularly: skin, bladder and lung cancers[10]. In addition, long-term ingestion of inorganic arsenic is linked to developmental effects, genetic mutations, infant mortality, neurotoxicity, diabetes, pulmonary disease and cardiovascular disease[11, 12] .

Lead Pb (II) is another dangerous heavy metal that occurs naturally in the environment with a density 5 times greater than that of water[13]. Human exposure to lead results from anthropogenic activities, industrial production and use, and domestic and agricultural use[14]. This led to their wide distribution in the environment; raising concerns over their potential effects on human health and the environment. Lead poisoning as arsenic is an environmental and public health problem of global proportions. World Health Organization (WHO) also considers lead one on the most serious environmental poisons among various heavy metals in the world and classified as human carcinogens according to the U.S. Environmental Protection Agency, and the

International Agency for Research on Cancer. According to the Food and Drug Administration (FDA) in the U.S the maximal lead level in water should not exceed $10 \mu\text{g l}^{-1}$ [15]. Thousands of communities around the world suffer lead exposure, and it has been reported that 120 million people around the world are overexposed to lead, mainly in Senegal, China and India. Currently, there is a huge research interest in experimenting alternative options to remediate lead pollution especially in industrial wastewater to meet technology-based treatment standards.

That being said, it is essential to reduce human intake of arsenic and lead especially from water to alleviate the impact of these heavy metals' contamination. For that purpose, many methods have been devised ranging from: oxidation, coagulation, ionic liquid solvents [16], solid phase extraction by covalent attachment, usage of different types of carbon nanotubes such as manganese dioxide-coated multiwall [17], usage of hybrids[18], ion exchange to membrane techniques and even phytoremediation.

Recent approaches involve phytoremediation that uses green plants to completely absorb and dissociate the pollutants from the environment[19], or rhizofiltration which utilizes the plants to adsorb, absorb, concentrate and precipitate metal from solution[20]. Results showed that within 60 minutes of exposure to a powder produced from dried roots more than 93% of arsenite and 95% of arsenate were absorbed[21].

Finally, the most popular and promising method used for arsenic and lead removal is adsorption owing to the high efficiency, low cost and ease in operation[6]. There are

many adsorbents reported in literature for the removal of As (V) such as: activated carbon, hydrated ferric oxide, activated alumina, iron and manganese coated sand, and other natural and synthetic materials[4]. There are also several adsorbents tested and reported for the removal of Pb (II) such as: activated carbon, hydrated ferric oxide, activated alumina, iron and manganese coated sand, and other natural and synthetic materials[4]. In most of the cases packed column or Fixed beds are used for the purpose of adsorption[22]. In a packed column of activated alumina for example, as water passes through, the impurities including arsenic present in water are adsorbed on the surfaces of activated alumina grains, hence large surface area and adequate adsorbent are essential for effective adsorption[23]. The arsenic and lead adsorption capacity of conventional adsorbents like activated carbons, and activated alumina is unsatisfactory; hence new adsorbents are being investigated, particularly the Metal-organic frameworks (MOFs)[24].

Metal-organic frameworks (MOFs) are some of the most important and recent discoveries in material science[25]. They are nanoporous solids made up of inorganic metal (or metal-containing cluster) coordinated to organic ligands[26]. Many features including tunable pore size, high internal surface area, thermal stability, and the exposed active sites were enough for the MOF to receive attention and to be used in many processes including gas storage, selective separation, catalysis, nanoscale drug loading and biochemical imaging[27]. Compared to the old solid adsorbents such as silica

materials, and activated carbon, MOFs are much more important and of great interest nowadays because of their great Features. With easy functionalization, MOFs become very effective in adsorption and especially adsorption of heavy metals from water[28]. They exhibited a high potential in removing heavy metals from water such as lead, mercury, and arsenic. Furthermore, the previous adsorbents were reported to have effects on high concentrations and not on ultra-low concentration of adsorbate. However, MOFs have shown high removal efficiency at the ultra-low concentrations level (ppb levels)[29].

In this thesis, zinc based metal organic frame work (Zn-MOF-74) will be investigated as an adsorbent agent for arsenic and lead removal. Zn-MOF-74 is environmental friendly and showed strong affinity towards arsenic and lead species by adsorbing As(V) and Pb(II) on its surface. Zn-MOF-74 is highly stable with very good chemical stability compared to thousands of other MOFs reported in the literature[30]. This is one of the reasons behind choosing this MOF specifically in water treatment. It is prepared at high temperature and at room temperature and by changing the route of preparation, the morphology and capacity changes. A series of characterizations were done on the Zn-MOF74 including scanning electron microscope (SEM), powder x-ray diffraction (PXRD), Thermo-Gravimetric Analysis (TGA), Brunauer-Emmet-Teller (BET), Fourier Transform infrared spectroscopy (FTIR), Zeta-Potential analyzer

CHAPTER II

LITERATURE REVIEW

Waste water treatment and the removal of heavy metals from water are significant issues targeted by many developing countries in the world. Many techniques have been used to remove heavy metals from water and below are the most recently used ones:

- Chemical oxidation and advanced oxidation
- Chemical Precipitation
- Chemical coagulation
- Chemical stabilization
- Ion exchange
- Membrane filtration
- Adsorption

A. Chemical Oxidation and Advanced oxidation

Chemical oxidation includes the introduction of an oxidizing agent to the wastewater, causing electrons to move from the oxidant to the pollutants, which goes modification in the structure and become less destructive[31]. Advanced oxidation, through processes

such as air stripping, steam stripping or activated carbon adsorption, can help remove any toxic byproducts obtained of chemical oxidation[31]. Advanced oxidation and chemical oxidation are usually used for the pretreatment of heavy metal wastewater containing organic compounds. The main problem of chemical oxidation is that it produces toxic byproducts.

B. Chemical Precipitation

Chemical precipitation is one of the main widely used techniques for the removal of heavy metals from inorganic effluent due to its simplicity[32]. It involves addition of precipitation reagent to the wastewater for the chemical reaction that converts the dissolved metals into solid particles to occur[32]. The mechanism of this process is based on the following: Insoluble metal precipitation by reacting dissolved metals in the solution are produced. During precipitation, very fine particles are generated and chemical precipitants, coagulants, and flocculants are used to increase their particle size to remove the particles as sludge[33]. However, this technique is not effective for treating wastewater with high acid content, and it produces a large quantity of toxic sludge that needs to be treated with chemical stabilization and disposed of properly.

C. Chemical Coagulation

This method is based on the zeta potential that identifies the electrostatic interaction between pollutants and coagulants agents[34]. It is always used following chemical precipitation, destabilizes fine solid wastewater particles so that they aggregate during chemical flocculation. The surfactants added in the coagulation process neutralizes the charge of the particles causing them to sediment to the bottom[35]. The particles are normally negatively charged, preventing them from forming larger groups and settling. Chemical coagulation introduces positively charged coagulants that reduce the negative particles' charge, enabling them to form larger groups. An anionic flocculants introduced to the mixture reacts against the positively charged mixture to bind the particles into larger groups, and can be removed by filtration or sedimentation[35]. The supernatant solution that is extracted will still have few particles dispersed in it and this means that the solution needs to be treated by extra processes.

This technique is not appropriate for treating wastewater with high acidic content because it is not acid resistant. Hence, the sediment contains heavy metals that need further treatments like neutralization or dehydration.

D. Chemical Stabilization

This process involves treating sludge which is a byproduct of chemical precipitation and chemical coagulation with an oxidant to decrease the rate of poisonousness that has grown within the sludge[36]. This method is usually used in lands where fertilizers are heavily used and hence where lead is highly concentrated. After that, the sludge is either incinerated or solidified to be disposed of later in the landfills.

E. Ion Exchange

Ion Exchange is a chemical reaction that in which heavy metal ions from wastewater are exchanged for a similarly charged ion attached to a solid particle[37]. As a cost efficient process, it has been proved to be also very effective in removing heavy metals from water even in very low concentrations and this what made ion exchange one of the most widely used methods in water treatment industry.

Ion exchange resins are water insoluble solid substances that can absorb both positively and negatively charged ions from the electrolyte solution[38]. After that, it releases other ions with same charge as the absorbed ones into the electrolyte solution with the same amount. Hence by this, the positively charged ions in cationic resins such as hydrogen and sodium ions are exchanged with positively charged ions, such as nickel,

copper and zinc ions, in the solutions[38]. At the same time, the negatively charged ions such as hydroxyl ions can be replaced by the negative ions such as sulfate and chromate. However, what makes this process not highly used is the limitation by the concentration and acidic levels of the waste water. If the wastewater used is highly acidic, it needs a pretreatment prior to using the ion exchange technique.

F. Membrane Filtration

Membrane filtration is a widely used method for the treatment of inorganic effluents that contains heavy metals. According to the size of the particle, many types of membrane filtration can be used such as ultra-filtration, nanofiltration, and reverse osmosis.

Ultrafiltration (UF) utilizes permeable membrane to separate heavy metals, macromolecules and suspended solids from inorganic solution according to the pore size and molecular weight of the separating compounds [31]. Depending on the membrane characteristics, UF can achieve more than 80% of removal competence with a metal concentration reaching from 15 to 130 mg/L at pH ranging from 4.5 to 9 and at 2–5.5 bar of pressure.

G. Adsorption

Adsorption is a process that occurs when a gas or liquid solute accumulates on the surface of a solid or a liquid (adsorbent), forming a molecular or atomic film (the adsorbate)[39]. Recently, numerous approaches have been studied for the development of cheaper and more effective technologies, both to decrease the amount of wastewater produced and to improve the quality of the treated effluent. Adsorption has become one of the alternative treatments, in recent years, the search for low-cost adsorbents that have metal-binding capacities has intensified[40]. The adsorbents may be of mineral, organic or biological origin, zeolites, industrial by-products, agricultural wastes, biomass, and polymeric material[41]. In general, there are three main steps involved in pollutant sorption onto solid sorbent: (i) the transport of the pollutant from the bulk solution to the sorbent surface; (ii) adsorption on the particle surface; and (iii) transport within the sorbent particle. Technical applicability and cost-effectiveness are the key factors that play major roles in the selection of the most suitable adsorbent to treat inorganic effluent. Different types of adsorbents already exist and are reported in the literature including: Industrial By Products, Modified biological and agricultural wastes, Modified biopolymers and hydrogels, Modified natural materials, and last but not least

Metal Organic Framework. The table below summarizes different adsorbents used for removing Arsenic and Lead from water in addition to their adsorption capacities.

Table 1: Reported adsorbents used for removing As(V) and Pb(II) from water.

Adsorbent	Adsorption capacity (mg/g)		Ref.
	As(V)	Pb(II)	
Boehmite-Alumina	20.7		[42]
Activated Carbon	3.09	54.1	[43, 44]
Fe(III)-Si	21.1		[45]
UiO-66	303		[46]
Maghemite	50		[47]
Iron Coated Zeolite	0.68		[48]
Calcined Phosphate		155	[49]
Modified Zeolite		123	[50]
Nostoc Species		93.5	[51]
Magnetite Fe ₃ O ₄	12.22		[52]
Activated Phosphate		4	[53]

Ecklonia maxima		235	[54]
-----------------	--	-----	------

All the above mentioned adsorbents were proved to be efficient on macro-scale only and haven't been used in adsorption experiments at the ultra-low levels while knowing that heavy metals exist in ultra-low concentrations in many areas in the world. Hence, the reported adsorbents weren't found to be industrially promising while the MOF adsorbents are and the main proof is the paper of removing mercury from water using Zn-MOF-74.

On a fundamental level, MOFs included the beauty of chemical structures and the power of combining organic and inorganic chemistry, two disciplines often regarded as disparate. Since the 1990s, this area of chemistry has shown a huge growth, as evidenced by not only the very high number of published papers about it also the ever-expanding trend of the research[55]. Although the number of review articles has also intensified in the last five years, we believe this thematic issue of Chemical Reviews, including the most up-to-date aids from leading MOF investigators all over the world, is necessary to mark the improvement made thus far in an inclusive manner. The scope of the volume ranges from topology analysis reaching to molecular simulations and synthesis, from

adsorptive material to catalysis and finally to applications in the biomedical fields[55]. As such, we hope that it will serve as an appreciated resource for new and present researchers in the field alike.

Many features makes the MOF special mentioning high internal surface area, tunable pore size, high thermal stability, and the exposed active sites were plenty for the MOF to receive courtesy and to be used in many processes including selective separation gas storage, catalysis, biochemical imaging and nanoscale drug loading [27]. Compared to the old solid adsorbents such as silica materials, and activated carbon, MOFs caught greater interest nowadays because of their exclusive features. With easy functionalization, MOFs become very effective in adsorption and especially adsorption of heavy metals from water[28].

Synthesis of the MOF has been playing a great role. By changing the root of the synthesis not only the morphology changes, but also the behavior and the characteristics of the MOF itself change. For example, the surface area of the MOF is highly affected by changing the experimental conditions while preparation. Among these developments, the following is fundamentally important: the ability to control the connectivity of vertices in a MOF structure, as well as the metrics and functionality of a given structure

without altering its underlying connectivity[32]. This allows for the control one needs to achieve many of the structures and properties discussed.

MOF-74 is one of the most highly stable metal organic framework that have discovered so far. It is made up of an inorganic metal with organic linker. The high chemical stability of this MOF made it more attractive for water treatment applications than the other thousands of reported MOFs until now[56]. It is a porous crystalline material with high surface area, thermal stability, and adsorption capacity[56]. Different inorganic metals can be used for precipitating the M-MOF-74 and “M” represents the metals that can be used for example Co, Ni, Mg, Zn.

MOF-74 have been used and reported in several applications. Co-MOF-74 showed both high CO₂ and water vapor sorption capacities (288 and 466 mg g⁻¹, respectively) and high selectivity against N₂ (>25) at 25 °C[57]. The synthesized Mg-MOF-74(S) crystals having Lewis acid sites (open metal sites) showed both high CO₂ and water vapor sorption capacities (350 mg g⁻¹ and 593 mL g⁻¹, respectively) at 298 K[58]. Fe-MOF-74 has been reported for C1–C3 Hydrocarbon Separation[59]. HT-Zn-MOF-74 has been reported for removing Hg²⁺ ions from water[60].

Further investigations have been made for choosing the best metal to use or even the best combination of metals and after several testing it was obvious that Zn-MOF-74 is the best one to be used in water treatment owing to its highest adsorption capacity, thermal and chemical stability[56].

Figure 1 below represents the crystal structure of Zn-MOF-74 where it has the form of honeycomb. Each zinc metal is connected to five oxygen atoms and has one open metal site.

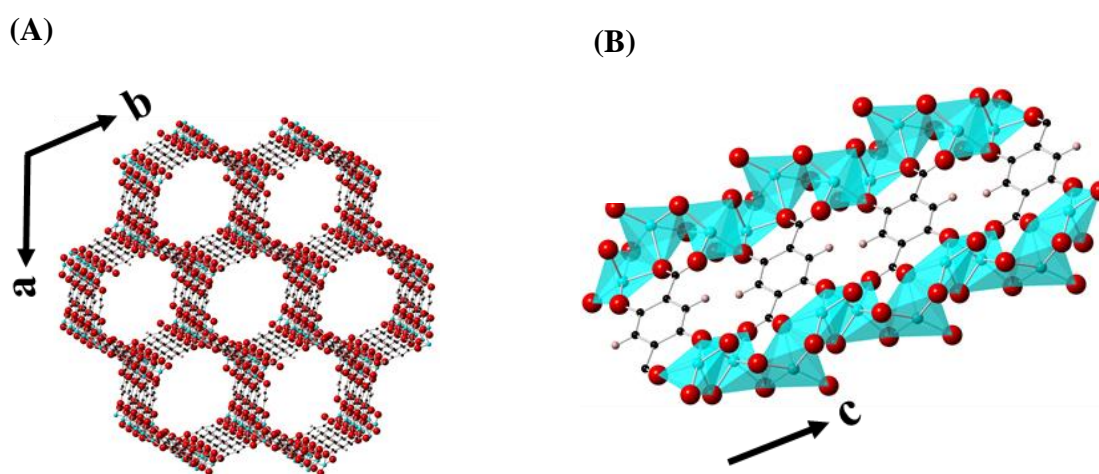


Figure 1. Crystal structure of Zn-MOF-74, view along c axis showing the honeycomb like pores; color code: C : black, Zn : blue, O : red, H : pink (A) coordination mode of zinc atom by DOT forming rod like secondary building units (B).

CHAPTER III

METHODOLOGY

A. Synthesis and Reagents

All used chemicals were of analytical grade and used without any purification. Zinc nitrate hexahydrate (98%, SIGMA-ALDRICH) and dihydroxyterephthalic acid (98%, SIGMA-ALDRICH) were used as the precursor salt and the organic linker, respectively. N,N-dimethylformamide (DMF) and ethanol were used as organic solvents to dissolve the reactants. Sodium arsenate (98%, SIGMA-ALDRICH) was used to prepare arsenic model samples. Na_3AsO_4 was dissolved in pure water to give As(V) stock solution. This solution was then diluted in pure water to prepare for the various batches of adsorption experiments.

Zn-MOF-74 crystals were prepared using two methods; room temperature precipitation and solvothermal procedure. For room-temperature synthesis, 0.081 g of 2,5-dihydroxyterephthalic acid and 0.19 g of zinc nitrate hexahydrate ($\text{Zn}(\text{NO}_3)_2 \cdot 6\text{H}_2\text{O}$) were dissolved in solution composed of 5 ml of DMF, 600 μL ethanol and 600 μL water. The solution was then left on magnetic stirrer at room temperature and after 1 min, 300 μL

of triethylamine (TEA) were added and kept on magnetic stirrer for another 1 hour after which the precipitates were collected by centrifuging the mixture. For the solvothermal procedure, the Zn-MOF-74 was synthesized by following a reported procedure [61, 62] where similar quantities, used for the room-temperature synthesis, of organic linkers and metal precursors were dissolved in a solution composed of 10 mL of DMF, 1 mL ethanol and 1 mL water, and the mixture was heated to 120 °C for 24 hours. The collected samples from the room temperature precipitation and solvothermal method were collected and washed with DMF and Dichloromethane (DCM) several time to ensure the purity of the synthesized MOFs.[60] RT-Zn-MOF-74 and HT-Zn-MOF-74 designate the MOF-74 synthesized at room temperature and at high temperature (120 °C), respectively (Scheme 1).

B. Characterization

For powder XRD (PXRD) analysis, the produced MOFs were dried after washing and inserted into a Bruker D8 discover XRD diffractometer which employs a Cu K α radiation ($\lambda = 1.5406 \text{ \AA}$) that operates at 40 kV and 40 mA, with 2θ ranging between 5° and 40° at a scanning rate of 0.3 ° min⁻¹ and a total analysis time of 180 min. The confirmation of the MOF structure was done by comparing the recorded PXRD pattern

with the simulated single crystal structure of MOF-74 reported in the literature. Thermal stability of the produced MOFs, thermogravimetric analysis (TGA), was also carried out on a TG 209 F1 Iris (Netzsch, Germany). The procedures included heating very few milligrams of the MOF sample in the presence of nitrogen from 30 °C to 1000 °C while the temperature ramp was constant and equal to 5 °C min⁻¹.

Nitrogen adsorption/desorption isotherms were measured using Micromeritics ASAP 2420 and Brunauer–Emmet–Teller (BET) equation was used to calculate the surface area. The prepared MOFs were activated by washing them for 3 days with DMF and further 3 days with DCM to ensure the removal of the unreacted starting materials from the MOF crystals. The samples were then activated via degassing at 120 °C overnight and finally N₂ adsorption/desorption isotherms were measured. The morphology of the prepared MOFs was studied using Scanning electron microscopy (SEM) and in order to account for possible aggregation resulting from preparation procedures. After washing and drying, a thin layer of gold (5 nm) was used to coat the MOFs sample and then it was inserted into a Tescan Mira SEM, operating at 5 kV with Oxford detector for energy dispersive X-ray (EDX) characterization to provide SEM photographs of the prepared MOFs.

C. As(V) Adsorption Experiments

The removal of arsenic by adsorption using RT-Zn-MOF-74 and HT-Zn-MOF-74 was studied using batch adsorption experiments. Room temperature was used as a standard temperature to all the adsorption experiments except for the experiment effect of temperature. The equilibrium adsorption capacity q_e (in mg g^{-1}) was obtained using the following equation:

$$q_e = \frac{(C_0 - C_e)}{m} \times V \quad (1)$$

where C_0 represents the initial concentration of As(V) (mg L^{-1}), C_e is the concentration of As(V) at equilibrium (mg L^{-1}), V is the volume of the aqueous solution (L), and m is the weight of MOF-74 (g).

For the adsorption kinetics, and the effect of pH and temperature experiments, 10 ml volume of the model solution (water and arsenic) was placed in a glass bottle and mixed with 10 mg of the each of the MOFs, separately, at a mixing rate of 200 rpm at room temperature. The initial concentration of arsenic was maintained at 40 mg L^{-1} (40 ppm). The kinetics experiments were carried out for 48 hours where multiple glass bottles were used to represent different time intervals. Similar procedures were used to study the effect of pH on the removal of arsenic and the pH of the solution was adjusted using 0.1 M HCl and NaOH.

For the thermodynamic analysis for the As(V) removal, a temperature range between 25 °C–45 °C was used. Adsorption isotherm experiments were performed using the same procedures employed for kinetic experiments except that the concentration range of arsenic was assorted from 5 mg L⁻¹ to 150 mg L⁻¹. For most of the samples, three replicate AA measurements were performed to ensure a standard error of less than 1% for each one. Arsenic concentration was measured using Thermo Labsystems, solar atomic absorption spectrophotometer (AA) with ASX-510 autosampler, and Solaar data acquisition.

D. Pb(II) Adsorption Experiments

The removal of Lead ions by adsorption using RT-Zn-MOF-74 and HT-Zn-MOF-74 was studied using batch adsorption experiments. All lead ions adsorption experiments were conducted at room temperature except for the effect of temperature experiments. The adsorption capacity at equilibrium q_e (in mg g⁻¹) was calculated using equation (1):

$$q_e = \frac{(C_0 - C_e)}{m} \times V \quad (1)$$

where C_0 is the initial concentration of Pb(II) (mg L^{-1}), C_e is the equilibrium concentration of Pb(II) (mg L^{-1}), V is the volume of the aqueous solution (L), and m is the weight of MOF-74 (g).

The experimental data were fitted to three isotherms namely: Langmuir, Freundlich, and Dubin Radushkieh (D-R) isotherms. Adsorption isotherms provide insights into surface properties, affinity of adsorbent, and adsorption mechanism. The Langmuir isotherm assumes a monolayer adsorption that describes the surface as energetically homogeneous and that a monolayer coverage is formed in addition to that no interactions occurs between the adsorbed species. Freundlich isotherm describes a heterogeneous surface and assumes that there is an intermediate interaction between the adsorbed molecules. Dubin Radushkieh (D-R) isotherm is usually applied to the adsorption process that occurs on both heterogeneous and homogeneous surfaces. The table below shows the linear and non linear forms of the three mentioned isotherms.

Isotherm	Linear Form	Nonlinear Form
Langmuir	$\frac{C_e}{q_e} = \frac{C_e}{q_m} + \frac{1}{k_1 q_m}$	$q_e = \frac{q_{\max} b C_e}{1 + b C_e}$
Freundlich	$\ln q_e = \ln k_1 + \frac{1}{n} \log C_e$	$q_e = K_F C_e^{1/n}$

Dubin Radushkieh	$\ln q_e = \ln q_s - \beta \varepsilon^2$	
	Where $\varepsilon = RT \ln(1 + \frac{1}{C_e})$	$q_e = q_s \exp(-\beta \varepsilon^2)$

In the table above, q_e (mg g^{-1}) is the amount adsorbed at equilibrium, C_e (mg L^{-1}) is the concentration of adsorbate at equilibrium, q_m is the maximum adsorption capacity, K_L (L mg^{-1}) is an equilibrium constant related to the binding strength; n and K_F (L mg^{-1}) are Freundlich constants that indicate the adsorption capacity and intensity, respectively. R is the universal gas constant ($8.314 \text{ J mol}^{-1}\text{K}^{-1}$), T is the absolute temperature, q_s (mol g^{-1}) is the theoretical monolayer adsorption capacity and β ($\text{mol}^2 \text{ J}^{-2}$) is the constant which is related to the mean sorption energy (E). The mean adsorption energy E (KJ mol^{-1}) gives information about the nature of the adsorption process whether it is physiosorption or chemisorption and it can be expressed using the following equation:

$$E = \frac{1}{\sqrt{2\beta}} \quad (2)$$

For the adsorption kinetics, and the effect of pH and temperature experiments, 10 ml volume of the model solution (water and lead) was placed in a glass bottle and mixed with 10 mg of the each of the MOFs, separately, at a mixing rate of 200 rpm at room

temperature. The initial concentration of lead was maintained at 100 mg L^{-1} (100 ppm). The kinetics experiments were carried out for 2 hours where multiple glass bottles were used to represent different time intervals. Similar procedures were used to study the effect of pH on the removal of lead and the pH of the solution was adjusted using 0.1 M HCl and NaOH.

For the thermodynamic analysis for the Pb(II) removal, a temperature range between $25 \text{ }^{\circ}\text{C}$ – $50 \text{ }^{\circ}\text{C}$ was used. Adsorption isotherm experiments were performed using the same procedures employed for kinetic experiments except the initial concentration of lead which was assorted from 10 mg L^{-1} to 700 mg L^{-1} . For most of the samples, three replicate AA measurements were performed to ensure a standard error of less than 1% for each one. Lead concentration was measured using Thermo Labsystems, solar atomic absorption spectrophotometer with ASX-510 autosampler, and Solaar data acquisition.

CHAPTER IV

CHARACTERIZATION OF Zn-MOF-74

Figure 2A depicts the PXRD patterns of the Zn-MOF-74 samples prepared using solvothermal and room temperature precipitation. It is clear that the synthesized compounds are highly crystalline and the peaks comply with the simulated ones[63], which indicate the high purity of the RT-Zn-MOF-74 and HT-Zn-MOF-74 samples. Nevertheless, a broadness in the main peaks of RT-Zn-MOF-74 sample can be noticed, which validates the formation of nanosized crystals as evidenced by the calculation of the particle diameter using the Scherrer's equation (66 nm for RT-Zn-MOF-74 and 144 μm for HT-Zn-MOF-74). After being exposed to water and with adsorbed arsenic on their surfaces, XRD patterns affirm that the crystallinity of Zn-MOF-74 is well-retained demonstrating the high stability of Zn-MOF-74 in water.

Thermogravimetric Analysis (TGA) is employed to study the thermal stability of Zn-MOF-74. The percent weight loss related to the synthesized MOFs is based on control samples that contains only MOFs. Figure 2B provides a relation between the percentage of MOF weight lost and temperature. As can be seen in the Figure 2B, considerable weight loss is observed below 200 °C for the as synthesized RT and HT-Zn-MOF-74 samples. Between 15–20% weight loss is seen in this range and this can be due to the evaporation of water and other solvents. At ca. 100 °C, while the coordinated water on

the metal center remains bonded, there are some weakly adsorbed water molecules inside the cavity that start to desorb. As the heating process continues, the water molecules coordinated originally to the metal sites starts to desorb at higher temperature almost (ca. 200 °C)[61]. Another major weight loss is observed between 200 °C–500 °C which corresponds to the decomposition of the MOFs and agrees with what has been reported in the literature[60]. Furthermore, after decomposition at 500 °C a total weight loss of 30%–40% of the initial weight is witnessed for the virgin MOFs. For the MOFs after the adsorption studies, it is clear from the TGA analysis that MOF-74 remains thermally stable at high temperature after the adsorption of As(V), and in the temperature range of 100 °C–200 °C the remaining residue from the used Zn-MOF-74 after adsorption is higher than that before adsorption. This is probably due to the presence of fewer guest anions in the MOF structure after adsorption.[60]

The surface areas for the RT and HT-Zn-MOF-74, evaluated by the BET method following degassing the sample at 120 °C, are found to be 690 m² g⁻¹ and 1201 m² g⁻¹, respectively (Figure 2C). The decrease in the BET surface area of the nanocrystalline RT Zn-MOF-74 is consistent with the reported values of BET surface area of M-MOF-74 (M=Zn, Mn, Mg, Co, Ni) which are found[64] to be ranging from 400 m² g⁻¹ to 1000 m² g⁻¹. The pore volume for the RT and HT-Zn-MOF-74 are found to be 0.826 cm³ g⁻¹ and 0.566 cm³ g⁻¹, respectively (Figure S1). The HT-Zn-MOF-74 isotherm is of type I

where the maximum quantity adsorbed is reached at low relative pressure while that of the RT-Zn-MOF-74 is of type IV. This can be explained by the use of triethylamine (TEA) as a reagent in the synthesis of RT-Zn-MOF-74, which can probably act as an etching agent for the wall of the pores by coordinating to the zinc cluster and therefore providing the mesoporous behavior to the MOF structure. Similar observations were also found in nano-sized Mg-MOF-74 using TEA, which competes with the terephthalate linkers.[65] In addition, the small particle size obtained at room temperature (less than 100 nm) introduces similar behavior in the adsorption of N₂ molecules.

SEM study has been carried out to understand and clearly see the structural features of the MOF crystals using both synthesis routes.

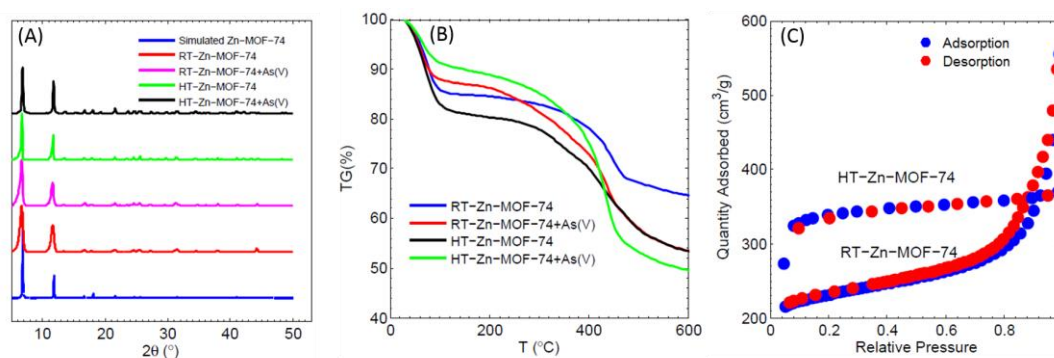


Figure 2. XRD Analysis of Zn-MOF-74 before and after adsorption of As(V) (A). TGA analysis of Zn-MOF-74 before and after adsorption of As (V) (B). N₂ Isotherms of RT-Zn-MOF-74 and HT-Zn-MOF-74 (C).

The obtained SEM images for RT and HT-Zn-MOF-74 are shown in Figure 3 and clearly exhibit that aggregation of particles resulted in both cases; however, the HT-Zn-MOF-74 particles have exhibited much higher levels of aggregation. The effect of aggregation might severely limit the adsorption capacity due to the reduction in the number of available adsorption sites.

Remarkably, the particles obtained at room temperature are small (less than 100 nm) while the particles obtained at high temperature are relatively larger crystals (more than 100 μm). These values are consistent with the calculated ones from PXRDs using the Scherrer equation.

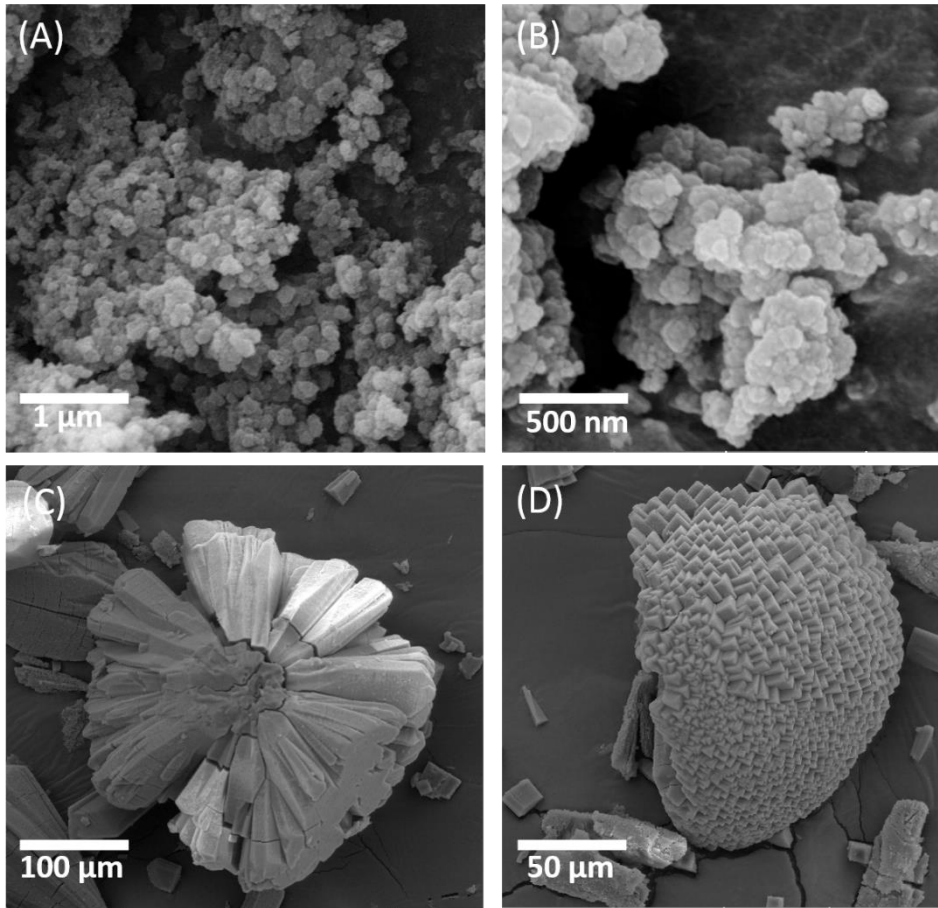


Figure 3. SEM images of RT-Zn-MOF-74 (A, B). SEM images of HT-Zn-MOF-74 (C, D).

CHAPTER V

ADSORPTION OF ARSENATE

Arsenate removal data for the HT-Zn-MOF-74 display much lower adsorption capacity, roughly 50% less than that of RT-Zn-MOF-74. This is believed to be due to the severe aggregation problems connected with the formation and use of HT-Zn-MOF-74. The nanosized MOF crystals should have more available adsorption and exposed sites than those in the large particles obtained via solvothermal technique. Indeed, the adsorption of As(V) on the surface of large particles results in an increase in the internal and external mass transfer limitations. Since the adsorption of As(V) is much higher for RT-Zn-MOF-74, the full adsorption study including the effect of pH and temperature, the thermodynamic and kinetic of the arsenic removal is performed on the RT-Zn-MOF-74 sample.

A. Effect of pH

The pH of the solution is very important in water treatment since it may affect the adsorption mechanism by altering the interaction of adsorbents and the adsorbates, mainly by controlling the surface charges and the ionization of the adsorbate in the

solution.[66] Arsenic, for example, exists in different forms in aqueous solutions at different pH values (speciation). It exists in the mono and deprotonated forms in the pH range of 2–10.[67] The effect of pH on the percent removal of arsenate using RT-Zn-MOF-74 is conducted in pH range of 2–10 as shown in Figure S2A. The percent removal efficiency of arsenate by RT-Zn-MOF-74, denoted by $R(\%)$, is shown to be dependent on the pH of the solution. At an initial arsenate concentration of 40 ppm, and adsorbents dosage of 1 g L^{-1} , around 80% removal can be achieved at pH around 7. The removal of arsenate using RT-Zn-MOF-74 is less effective in very acidic and basic solutions. Moreover, the percent removal efficiency increases from ca. 50% to ca. 80% when the solution pH is increased from 2 to 8. Its important to mention that Zn-MOF-74 is unstable at low pH and therefore no experiment was done at pH lower than 2. As Figure S2A depicts, the maximum removal of arsenate is acheived at pH value between 6 and 8. Two adsorption mechanisms can be investigated to elucidate the mechanism of adsorption: Electrostatic interactions or chemical reaction between the arsenate molecules and the functional groups on the surface of the RT-Zn-MOF-74[68]. We believe that the mechanism of adsorption of arsenate onto RT-Zn-MOF-74 is effectively due not only to chemical interactions that lead to the substitution of water molecules inside the pore channels by the arsenate anions.

The FTIR spectra in Figure S3 show medium broad band at 3400 cm^{-1} due to $\nu(\text{OH})$ which is expected for MOF-74 materials owing to their high hygroscopic character.

Interestingly, it can be seen that all functional groups originally present on RT and HT-Zn-MOF-74 are intact even after arsenate adsorption and are thus available for interaction with the metal ions.

B. Effect of temperature

Studying the effect of temperature on arsenate adsorption is extremely important. For example, polluted water from different industries are released over different temperatures depending on the process that they are generated from. The temperature effect on the adsorption isotherm is presented in Figure S2B. The increase in the temperature from 20 °C to 40 °C enhances the percent arsenate removal from 77% (30.8 mg g⁻¹) to 93% (37.2 mg g⁻¹). This reflects the endothermic nature of the arsenate adsorption on the surface of the RT- Zn-MOF-74. The reason behind the increase in the adsorption capacity with the increase in temperature might be related to the presence of strong interaction forces between the arsenate molecules and RT- Zn-MOF-74 particles. In this paper, we chose to work at 30 °C which still shows a high removal (85%) but closer to ambient temperature than 40 °C.

C. Adsorption kinetics

The effect of contact time on the adsorption of As(V) by RT- Zn-MOF-74 is depicted in Figure 4A. The remaining concentration of As(V) in the solution decreased as adsorption time increases, which lowers the static driving force of mass transfer. Thereby, the adsorption is rapid at the beginning when concentration gradient is high, and after 30 minutes, as the system approaches equilibrium, adsorption becomes slower. Equilibrium is established after 60 minutes and the adsorption capacity at equilibrium is calculated to be 36.1 mg g^{-1} . The adsorption kinetics are considered rapid in comparison with typical adsorbents[69] and this can be explained by the fact that the ultra-dispersion of sorbent particles leads to lower external mass transfer limitations.[70]

The mechanism of the adsorption processes whose limiting step might involve adsorption on a surface, chemical reactions or transport through diffusion is explored by studying the parameters extracted from the following kinetic models. Pseudo first-order and pseudo second-order kinetic models are the most common models used to analyze adsorption kinetics. A pseudo first-order kinetic model suggests that the rate of change in the solute concentration with time and the changes in the concentration of the adsorbate and the amount of adsorbent over time are logarithmically proportional.[71] On the other hand, a pseudo second-order kinetic model assumes that the adsorption capacity is proportional to the number of active sites occupied on the adsorbent. The

pseudo first-order[60] (Eq. 3) and pseudo second-order[72] (Eq. 4) model equations are given as follow:

$$\ln(q_e - q_t) = \ln q_e - k_1 t \quad (3)$$

$$\frac{t}{q_t} = \frac{1}{k_2 q_e^2} + \frac{t}{q_e} \quad (4)$$

where q_e (mg g^{-1}) is the capacity at equilibrium calculated experimentally, q_t (mg g^{-1}) is the amount adsorbed at time t , k_1 (min^{-1}) and k_2 ($\text{g mmol}^{-1} \text{min}^{-1}$) are the pseudo-first-order rate and pseudo second-order rate constants respectively. The results of the kinetic adsorption studies are shown in Figure 4B,C. Table 1 provides the obtained kinetic materials.

Table 2: parameters of As(V) adsorption kinetics by Zn-MOF-74.

Kinetic Model	Parameter	Value
Pseudo-First-Order	q_e (g mg^{-1})	21.9
	k_1 (min^{-1})	6.1×10^{-2}
	R^2	0.997
Pseudo-Second-Order	q_e (g mg^{-1})	38.7
	k_2 ($\text{g mg}^{-1} \text{min}^{-1}$)	4.3×10^{-3}

 R^2 0.993

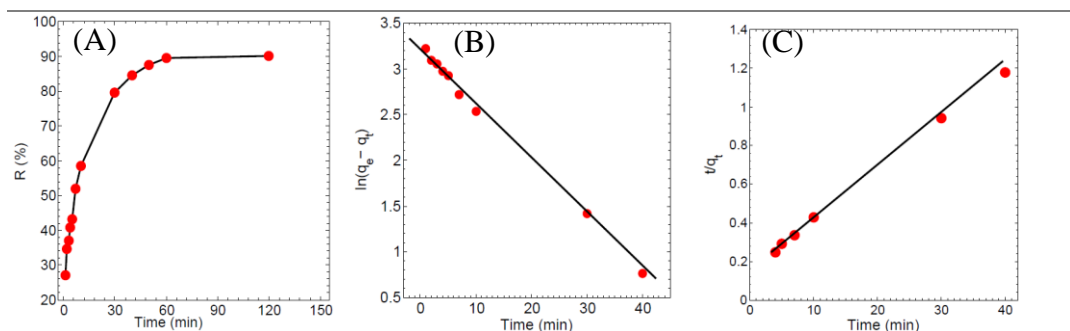


Figure 4. Effects of contact time on the removal of As(V) by the adsorbent Zn-MOF-74. $C_0 = 40 \text{ mg L}^{-1}$, $V = 10 \text{ mL}$, $m = 10 \text{ mg}$ (A). Pseudo first-order kinetics of As(V) removal by Zn-MOF-74 (B). Pseudo second-order kinetics of As(V) removal by Zn-MOF-74 (C).

According to the correlation coefficient (R^2) it can be concluded that the kinetics of arsenate adsorption on Zn-MOF-74 followed the pseudo first-order model. Nonetheless, the calculated capacity by pseudo-second-order (37.03 mg g^{-1}) is closer to the experimental value (36.1 mg g^{-1}) than that of the pseudo first-order (21.92 mg g^{-1}). Therefore, both physisorption and chemisorption mechanisms for the adsorption of As(V) on Zn-MOF-74 should be considered. Although Pseudo first-order and pseudo

second-order models can successfully provide the overall rate of adsorption process; however, the two models cannot predict whether internal or external diffusion is the rate limiting step during the adsorption. As a result, intra-particle diffusion model is used in order to analyze the rate controlling step using kinetic data.

Intra-particle diffusion model[73] at which the amount adsorbed at time t (q_t) can be written as:

$$q_t = k_{id} \cdot t^{1/2} + \theta \quad (5)$$

where k_{id} is the intra-particle diffusion rate constant ($\text{mg g}^{-1/2} \text{min}^{-1/2}$), and θ is a constant correlated to the thickness of the boundary layer (mg g^{-1}) and when the value of θ is large, the boundary layer effects becomes greater.[74] As shown in Figure S4, the adsorption process is described by three linearity plots, suggesting that three diffusion steps occur in the transport process of arsenate on RT-Zn-MOF-74 nanoparticles[75]. The first step is the transfer of arsenate molecules from the boundary film to the surface of RT-Zn-MOF-74, after which arsenate molecules transfer from the surface to the intraparticle active site and finally the diffusion of arsenate molecules on the active or binding sites of RT-Zn-MOF-74 until saturation is achieved. Using the intra-particle diffusion model, the rate constants of the three linear steps (the slope of the linear plots) are calculated and found to be 5.75, 1.72, 0.0631 for the first, second and third linear plots, respectively. Therefore, the external diffusion is the quickest step

whereas the intraparticle diffusion is thereby the rate controlling step during the adsorption process.[76]

D. Adsorption isotherm

The arsenate adsorption isotherms onto RT-Zn-MOF-74 are studied at pH 7.8 and temperature of 30 °C as it is found to be the optimal conditions. 10.00 mg of adsorbent are added to 10.00 ml aqueous samples (pH = 7.8) of adsorbate with different arsenate concentrations ranging between (5 mg L⁻¹–150 mg L⁻¹) at temperature $T = 30$ °C. The adsorption capacity of both RT-Zn-MOF-74 and HT-Zn-MOF-74 increases as the amount of As(V) in the sample solution increases as shown in Figure S5. This expected trend is due to the fact that a larger concentration gradient (the driving force of mass transfer) leads to the availability of more arsenate molecules in the vicinity of the active sites on the surface of the MOF particles. The experimental maximum adsorption capacity represented by the saturation point of both RT and HT-MOF-74.0 are 81.7 mg g⁻¹ and 45.1 mg g⁻¹, respectively. Furthermore, the data are evaluated using the following linearized Langmuir (6) and Freundlich (7) isotherms:

$$\frac{C_e}{q_e} = \frac{C_e}{q_{max}} + \frac{1}{k_1 q_{max}} \quad (6)$$

$$\ln q_e = \ln k_1 + \frac{1}{n} \log C_e \quad (7)$$

where q_e (mg g^{-1}) is the adsorption capacity at equilibrium, C_e (mg L^{-1}) is the equilibrium concentration of adsorbate, q_{max} is the maximum adsorption capacity, K_L (L mg^{-1}) is an equilibrium constant that represents the binding strength; K_F (L mg^{-1}) and n are Freundlich constants that indicate the intensity and adsorption capacity, respectively. The experimental data for both MOFs are fitted with Langmuir and Freundlich models and plotted in Figure 5, and the parameters of the best fits are summarized in Table 2. Based on the higher correlation coefficients (R^2) criterion, the Langmuir isotherm is found to fit the adsorption experiments of both RT-Zn-MOF-74 and HT-Zn-MOF-74 with maximum adsorption capacities, q_{max} , of 99.0 mg g^{-1} and 48.7 mg g^{-1} , respectively. A previous study on the adsorption of mercury(II) using HT-Zn-MOF-74 reported a close value of maximum capacity (63 mg g^{-1}).^[60] Our nanosized MOF removes twice as much arsenic from water under the same experimental conditions. In fact, the adsorption capacity of RT-Zn-MOF-74 is higher than many other adsorbents used and reported in the literature for removing As(V) at neutral pH including zirconium oxide (45 mg g^{-1})^[77], Iron(III)-loaded chelating resin (70 mg g^{-1})^[78], Iron(III) oxide-loaded melted slag (57 mg g^{-1})^[79], titanium dioxide (30 mg g^{-1})^[80], calcined mesoporous silica (11 mg g^{-1})^[81]. These results demonstrate the importance of particle size control for the adsorption processes.

Table 3: The Langmuir and Freundlich parameters and correlation coefficients for arsenate adsorption onto RT-Zn-MOF-74 and HT-Zn-MOF-74.

Model	Parameters	(RT-Zn-MOF-74) @ 30 °C	(HT-Zn-MOF-74) @ 30 °C
Langmuir isotherm	q_{\max}	99.0	48.7
$q_e = \frac{q_{\max} b C_e}{1 + b C_e}$	b	1.1×10^{-1}	3.5×10^{-2}
	R^2	0.953	0.964
Freundlich isotherm	K_F	17.3	1.20
$q_e = K_F C_e^{1/n}$	1/n	0.41	0.45
	R^2	0.933	0.959

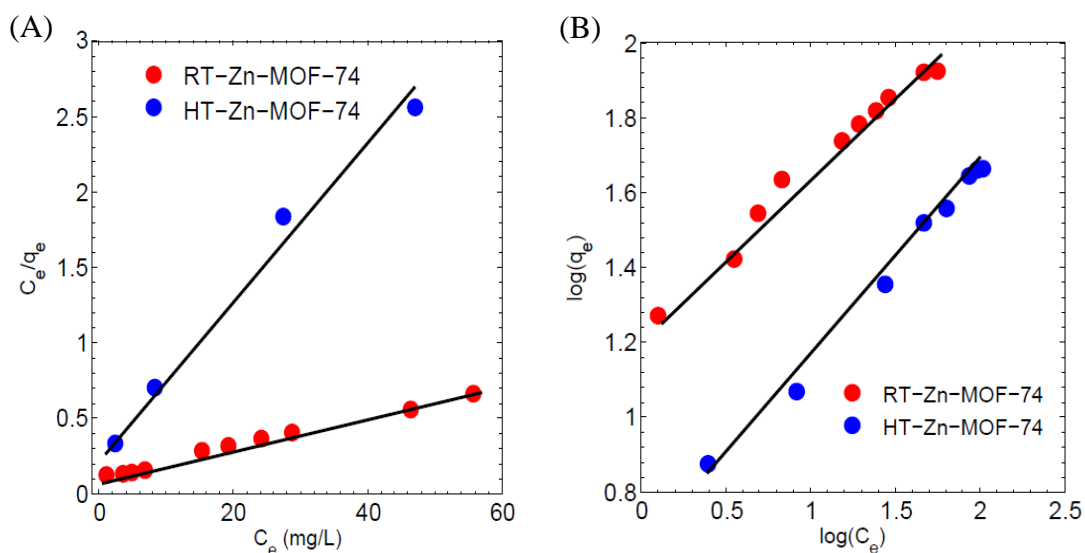


Figure 5. Langmuir isotherm for As(V) adsorption onto RT-Zn-MOF-74 and HT-Zn-MOF-74 (A). Freundlich isotherm for As(V) adsorption onto RT-Zn-MOF-74 and HT-Zn-MOF-74 (B).

Removal of ultra-trace As(V). RT-Zn-MOF-74 can also be considered as a promising adsorbent for the removal of ultra-trace (ppb) arsenate from water, especially that the threshold concentration of arsenic in drinking water is at 10 ppb.[6] To test this promise, similar procedures employed above are used with an initial arsenate concentration of 40 ppb and adsorbent masses varying between 2 mg and 20 mg. The highest removal in the ppb range is obtained for the case of 5 mg as shown in Figure 6. The removal percentage is also compared with an initial arsenate concentration of 40 ppm for the same mass of adsorbent. For example, lowering the mass from 10 mg to 5 mg results in

improving the removal percentage from 57% ($22.8 \mu\text{g g}^{-1}$) to 68% ($54.4 \mu\text{g g}^{-1}$). This might be attributed to the negative aggregation effect, which becomes more pronounced in the ppb range and that can be diminished by decreasing the mass of the adsorbent to a certain extent.[82]

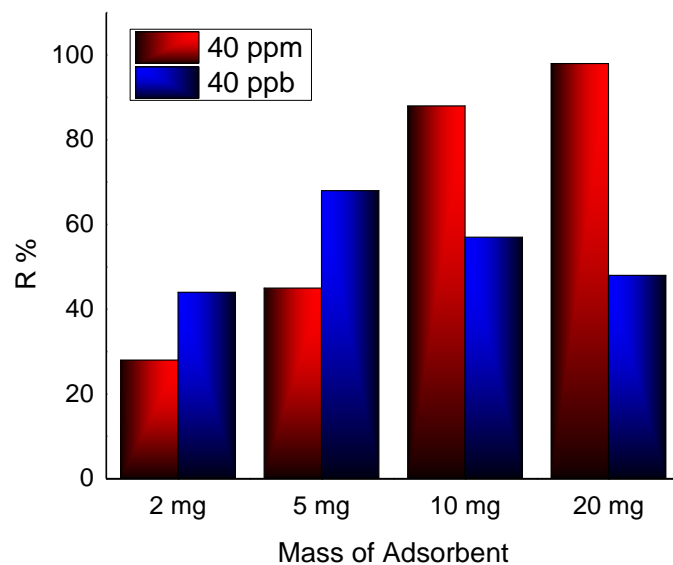


Figure 6: Effects of the mass of adsorbent RT-Zn-MOF-74 on the removal efficiency of As(V). pH = 7.8, T = 30 °C, t = 1 hr.

Moreover, several regeneration experiments for the used Zn-MOF-74 have been performed using a combination of NaCl, HCl, and Ethanol. The best recycling result was achieved by using about 0.1 mM HCl in ethanol, and 40% removal efficiency was obtained after the second adsorption cycle for 10.0 mg of used adsorbent and 50 ppm

As(V) original solution (Figure S6). The noticeable decrease in the adsorption capacity after reuse needs to be further optimized.

E. Thermodynamic Analysis

To provide better explanation for the nature and mechanism of the arsenate adsorption onto RT-Zn-MOF-74 surface, adsorption data at various temperatures, are used to find the thermodynamic parameters of adsorption such as change in standard free Gibbs energy (ΔG^0), change in standard enthalpy (ΔH^0), and change in standard entropy (ΔS^0). The thermodynamics of arsenic removal by the adsorbent RT-Zn-MOF-74 is assessed using the following Van't Hoff equation (Eq. 8) [83], at four different temperatures:

$$\ln(K) = -\left(\frac{\Delta H^0}{R}\right)\frac{1}{T} + \frac{\Delta S^0}{R} \quad (8)$$

where K is equilibrium constant computed as the ratio $K = q_e/C_e$ ($L\ g^{-1}$). Figure S7 represents the Van't Hoff plot and Table 3 contains the values of the aforementioned thermodynamic parameters including the Gibbs free energy at each of the 4 temperatures ($\Delta G^0 = \Delta H^0 - T\Delta S^0$).

Table 4: Thermodynamic parameters at T = 20 °C, 30 °C, 35 °C and 40 °C.

ΔH^0 (kJ mol ⁻¹)	ΔS^0 (J mol ⁻¹)	ΔG^0 (kJ mol ⁻¹)
K)		

		293 K	298 K	303 K	313 K
46.2	184.7	-2.94	-3.86	-4.78	-6.62

The positive value of ΔH^0 confirms and assures the endothermic nature of the adsorption of arsenate onto RT-Zn-MOF-74. On the other hand, spontaneity of the adsorption is assured by the negative values of ΔG^0 . The positive value of 46.2 kJ mol⁻¹ at 30 °C for ΔH^0 is most probably due to chemisorption consisting of the dehydration process of the metal atom and its environment, as discussed in the section on the TGA analysis, and the concomitant substitution with the arsenate. It has been established that there are several water environments in MOF-74, and upon heating the removal of the water molecules usually spreads from the center of the channels where they are weakly adsorbed towards the channel walls, where they are strongly coordinated to the metal.[61] In this last case, the metal atom, in its solvated state, is six-coordinated where one bond belongs to a single water molecule while the coordination sites that remained are filled with oxygen atoms belonging to the organic linker. Such dehydration step, which involves a transition from an octahedral structure into a five-coordinated square pyramidal, is more favored at higher temperatures. Therefore, the reported endothermic process is clearly due to the substitution of the various water molecules, including the one bound to the metal, by the arsenate anion, which becomes more favored as temperature is increased. This will be further investigated in the following section.

Moreover, the positive value of ΔS^0 suggests an increased randomness at the solid/solution interface with an increase in the degree of freedom of the adsorbed arsenate and could imply that the aforementioned dehydration mainly occurs at the pore center and away from the metal cluster of the MOF crystal, as corroborated by the TGA data and the intra-particle diffusion model.

F. Adsorption Energies via DFT Calculations

In order to better understand the experimental thermodynamic data of the adsorption of arsenate on Zn-MOF-74, solid-state DFT energy and geometry calculations are performed. As previously described, Zn-MOF-74 consists of zinc atoms coordinated to the organic linker 2,5-dihydroxyterephthalic acid (DOT). Each Zn^{2+} is coordinated to five oxygen atoms from the linker in a configuration close to the square pyramidal one. This configuration leaves an open metal site which can act as Lewis acid endowing MOF-74 with its good adsorption character. Therefore, when MOF-74 is in contact with water, the water molecules act as a Lewis base and coordinate to the Zn^{2+} open sites forming a primary layer. After saturation of the open metal sites, the excess water molecules form hydrogen bonds with the primary adsorbed water (P) and with the linker's oxygen atoms as shown in Figure 7. The adsorption energies of primary water molecules on the open sites are calculated and found to be -58 kJ mol^{-1} , while the adsorption energy of the secondary water (S) molecules is found to be -50 kJ mol^{-1} . These values for the water

adsorption enthalpies and for the bond distances (Figure 7) coincides with previously reported work.[84] On the other hand, in the presence of the adsorbate monodeprotonated arsenate ions (H_2AsO_4^-), the adsorption energy on the open sites is calculated to -91 kJ mol^{-1} (Figure 7). This value, which is more negative than that of water, indicates that arsenate is a stronger Lewis base than water and this is probably due to the negative charge of the arsenate ions. In other words, the adsorption of the arsenate molecules is thermodynamically more favourable than that of the primary water molecules as shown in the energy diagram in Figure 7. Therefore, in order for the arsenate to reach the open metal site, the water molecules in its vicinity has to be removed first. In the case of only two layers of water, the energy cost of this process is the sum of the two binding energies for primary and secondary water molecules reported above and is equal to -108 kJ mol^{-1} . This value is incompletely compensated by the -91 kJ mol^{-1} adsorption energy for the arsenate leading to an overall positive adsorption enthalpy of $+19 \text{ kJ mol}^{-1}$. Consequently, the more water layers are included, the more positive the enthalpy of adsorption, which is consistent with the value obtained experimentally of 46 kJ mol^{-1} as reported above. It is noteworthy that the difference between ΔE and ΔH for our system is small because it involves solids and liquids.

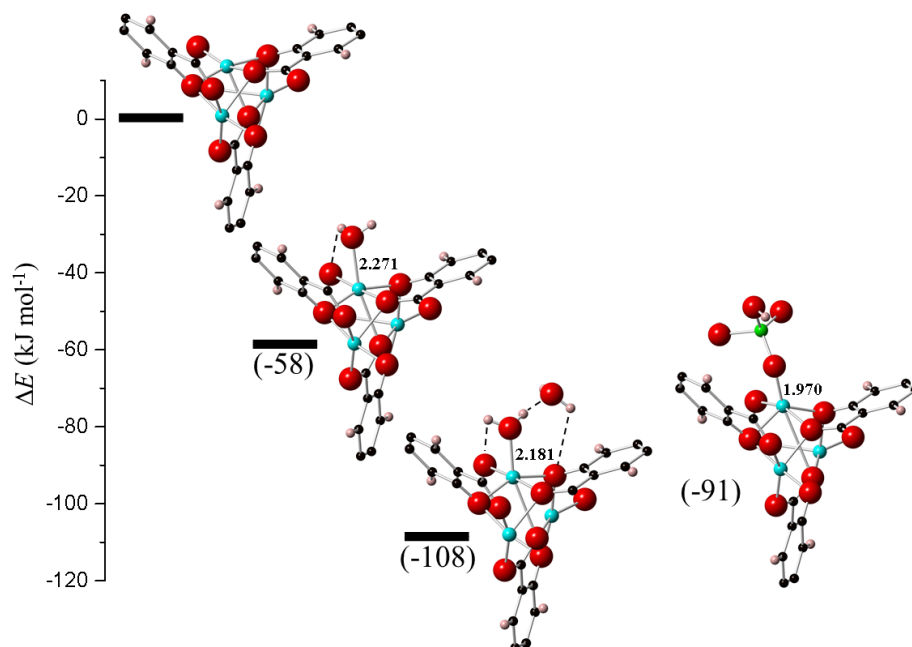


Figure 7. Energy level diagram of the adsorption of water and arsenate on Zn-MOF-74. In the primary adsorbed water (P), the distance between the O and Zn is 2.271 Å. When a second water is added this distance shortens to 2.181 Å. This bond strengthening is due to the hydrogen bonding between the hydrogen of the primary water and the oxygen of the secondary water (S). In addition to the hydrogen bonding between the secondary water and the O of the Zn-MOF-74 framework. On the other hand, the distance is shortest between the O of the arsenate and Zn (1.970 Å).

CHAPTER VI

ADSORPTION OF LEAD IONS

Lead (Pb (II)) removal data for the RT-Zn-MOF-74 display much higher adsorption capacity, roughly double that of HT-Zn-MOF-74. The reason behind this is the fact that severe aggregation problems are caused with the formation and use of HT-Zn-MOF-74. The large particles of the MOF obtained Solvothermally exhibits less exposed and active sites than those in the nano-sized crystals obtained via room temperature technique. Indeed, the adsorption of Pb(II) on the surface of large particles results in an increase in the internal and external mass transfer limitations. Because RT-Zn-MOF-74 have shown superb removal efficiency, the full adsorption study including the effect of pH and temperature, the thermodynamic and kinetic of the lead removal is performed on the RT-Zn-MOF-74 sample.

A. Effect of pH on lead adsorption and RT-Zn-MOF-74 nanoparticles surface charge

The removal efficiency of metal ions from aqueous solution highly depends on the pH of the solution, where changing the pH affects the charge on the adsorbent surface and

the degree of ionization and speciation of the adsorbates. Many of the research papers that were conducted on heavy metals adsorption indicated that the decrease in the ion uptake from the solution at acidic pH might be due to the increase in the competition with protons on the active sites of adsorbent. At alkaline pH, however, different effects may arise due to other processes such as the predominant presence of hydrated species of heavy metals, changes on the surface and precipitation of the appropriate salts. In order to see the effect of changing pH on the adsorption of Pb(II) using RT-Zn-MOF-74, experiments were done by varying pH from 2 to 10 with an initial Pb(II) concentration 100 ppm. Figure 7 (A) represents the results obtained for the adsorbent.

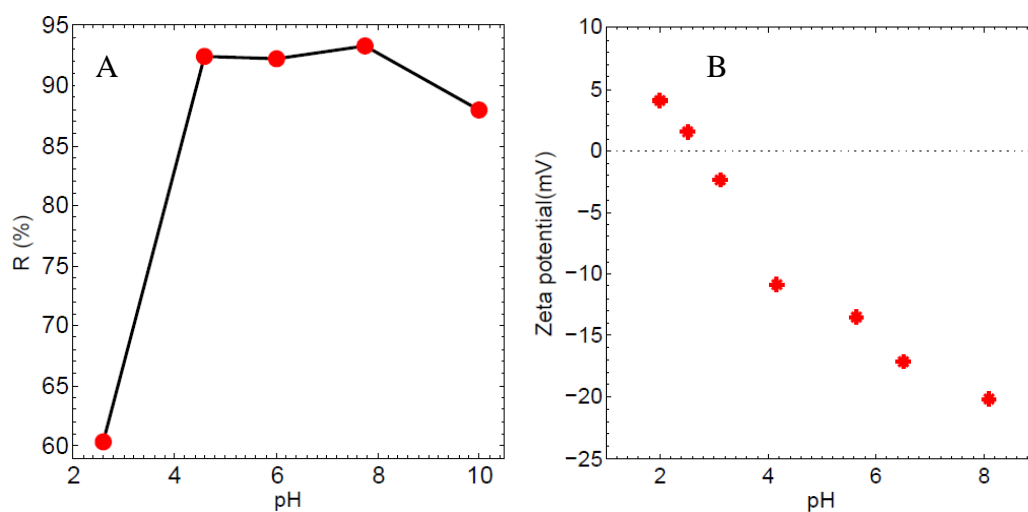


Figure 8: Effect of pH on the removal efficiency of Pb(II) ions (A). Effect of pH on the zeta potential of RT-Zn-MOF-74 (B).

Initially, as the pH increases from 2.5 to 4.2, the removal efficiency (R%) increases from 60% up to 93%. The very low uptake in the highly acidic medium range is due to the rise of competition between Pb^{++} ions and H^+ ions on the active sites of the adsorbent surface. The removal efficiency becomes almost steady within the pH range of 4.3 to 7.9 at a 93% to then drop again after $\text{pH}=7.9$. The decrease in the removal efficiency after $\text{pH}=7.9$ is due to the formation of hydroxyl complexes. It might be that OH^- in the basic medium affects firstly hydrolysis products of $\text{Pb}(\text{OH})^+$, and the $\text{Pb}(\text{OH})_2$ hydrolysis complexes. $\text{pH}=4.3$ which is the pH of the original 100 ppm $\text{Pb}(\text{II})$ solution is considered as the optimum pH with a removal efficiency of 93%.

In addition, solution pH can influence both the distribution of the lead species and binding sites of the RT-Zn-MOF-74. The determination of the isoelectric point (pH_{IEP}) or the point of zero charge of the adsorbent can help in optimizing the conditions needed for the adsorbent to give the maximum removal efficiency. Figure 7 (B) represents the relationship between the zeta potential of RT-Zn-MOF-74 and solution pH. As it can be seen from the figure, the pH_{IEP} of the adsorbent is 2.8 where the surface charge becomes zero. When the pH is greater than the pH_{IEP} , the surface of the adsorbent is negatively charged and when the pH of the solution is less than pH_{IEP} , the surface becomes positively charged. The results obtained from the zeta potential curve coincides with the results obtained in figure 7 (A) where the removal efficiency of Pb^{2+} ions decreases sharply from 93% to 60% when the pH of the solution decreases from

4.3 to 2 and this is due to the electrostatic repulsion that occurs between the positive Pb^{2+} ions and the positively charged adsorbent surface within this pH range.

B. Effect of adding salts to the solution on the removal efficiency of Pb(II)

Considering industrial wastewater, it contains in addition to heavy metals other organic and inorganic compounds such as salt ions. These compounds are expected to compete with the lead ions on the active sites of the adsorbent. For this reason, the effect of the presence of Sodium Nitrate, and Sodium bicarbonate on lead ion removal from aqueous solutions containing an initial lead ion concentrations of 80, 100, 120, 150, and 200 ppm onto RT-Zn-MOF-74 was investigated. The concentrations of Sodium nitrate and sodium bicarbonate were chosen to be 10 ppm and 150 ppm respectively which are relatively close to the normal concentrations at which these ions exist. Figure 8 depicts that the addition of sodium bicarbonate didn't affect much the adsorption efficiency while sodium nitrate did. When the initial lead concentration in the solution containing no added salts was 150 mg L^{-1} , the removal efficiency was 95.4% (143.1 mg g^{-1}). This percentage have dropped 90.7% (136.1 mg g^{-1}) after adding sodium nitrate to the solution while it remained almost the same by adding sodium bicarbonate.

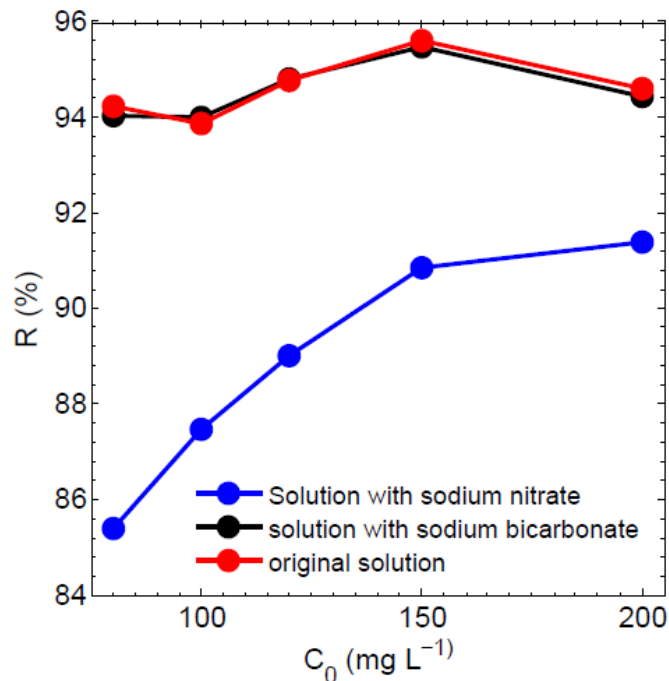


Figure 9: Effect of adding salts to the solution on the removal efficiency of Pb(II).

C. Effects of contact time and Temperature

It is very important to study the effect of temperature on the removal efficiency of lead ions because in industrial effluents the discharged materials leaves at various temperatures. In this study, 5 different temperatures were used (25, 30,35,40,50 °C) and the effect on the removal efficiency is shown in figure 9 (A) . As the temperature increases from 25 °C to 50 °C, the removal efficiency increases slightly from 93.2% to 96.3%. The uptake is very high on almost all the 5 temperatures ranges and the slight increase in the efficiency is due to the surface expansion of the nano materials upon

increasing the experimental temperature. When the adsorbent surface expands, the overall surface area available for adsorption increases leading to higher uptake and removal efficiency[85].

A series of contact time experiments were done at an initial lead(II) ions concentration of 100 mg L^{-1} and temperature and pH 30°C and 4.7 respectively. It is obvious from figure 9 (B) that as the time increases, the removal efficiency of lead ions increases to reach equilibrium after almost 90 mins. The adsorption of lead ions on RT-Zn-MOF-74 is considerably very quick where more than 90% removal efficiency was accomplished within the first 30 mins compared to many other adsorbents reported in the literature for removing Pb(II) ions[86-88]. The slope of the curve was very high within the first 30 mins and this is because of the high concentration gradient at the beginning of the experiment. After the first 30 mins the concentration gradient decreased leading to a decrease in the rate of mass transfer from the bulk of the liquid to the film layer of the adsorbent.

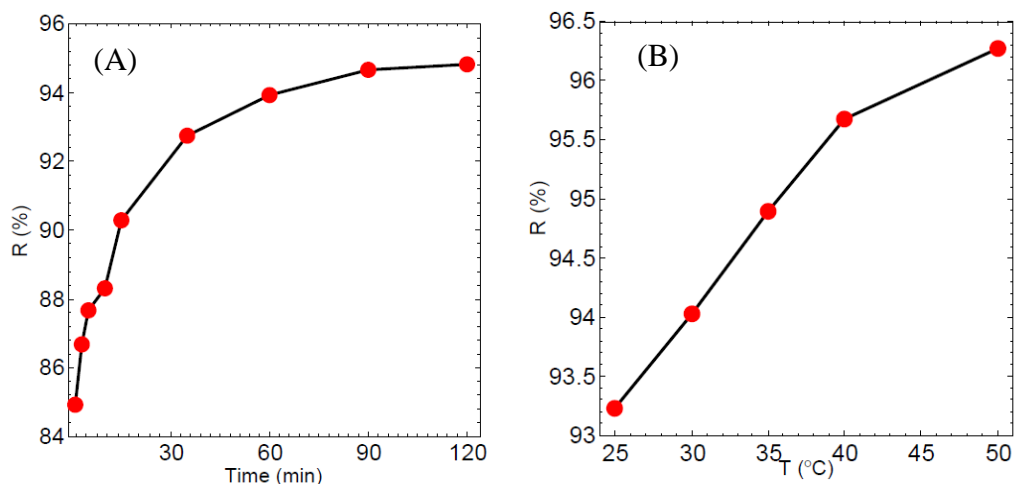


Figure 10: Effect of contact time on the removal efficiency of Pb(II) ions (A). Effect of temperature on the removal efficiency of Pb(II) ions (B).

D. Effect of Particle size

Figure 10 shows that the percent removal of Pb(II) increases from 47 to 94% as the particle size decreases from 144 μm to 66 nm for an initial concentration of 100 mg L^{-1} Pb(II) solution. The extent of the adsorption process increases with increased specific surface area. The specific surface available for adsorption will be greater for smaller particles and hence percent removal of metal increases as particle size decreases. For larger particles the diffusional resistance to mass transport is higher and most of the internal surface of the particle may not be utilized for adsorption. Consequently the amount of Pb(II) adsorbed is small[83].

E. Adsorption Isotherm

Figure 12 shows that the adsorption data of both RT and HT Zn-MOF-74 were successfully described by the three models with $R^2 > 0.95$ for all the adsorption isotherms (Freundlich, Langmuir, and DR) (Table 5).

Table 5: The Langmuir, Freundlich, and R-D parameters and correlation coefficients for Lead adsorption onto RT-Zn-MOF-74 and HT-Zn-MOF-74.

Isotherm	Parameter	Nonlinear Fitting		Linear Fitting	
		RT-Zn-MOF-74	HT-Zn-MOF-74	RT-Zn-MOF-74	HT-Zn-MOF-74
Freundlich	K	4.52	0.596	4.63	0.636
	n	1.713	0.774	1.723	0.798
	R^2	0.972	0.946	0.969	0.952
Langmuir	q_m	487	329.13	476.19	333.31
	K_l	0.0447	9.86×10^{-3}	0.0465	9.93×10^{-3}
	R^2	0.995	0.996	0.9945	0.9976
D-R	$\beta (\times 10^{-2} \text{ mol}^2/\text{Jol}^2)$	4.92	87.47	5	90

q_s (mg g ⁻¹)	244.8	163.33	248.38	161.92
E (KJ mol ⁻¹)	1.008	0.24	1	0.235
R ²	0.9942	0.9543	0.9945	0.956

The values of n obtained by Freundlich isotherm helps in checking the favorability of the process. In the case of RT-Zn-MOF-74, the values of n obtained by linear and non-linear fitting are higher than 1 (1.72, 1.71) respectively. This indicates that the adsorption is normal and the process is favorable[89]. While for the HT-Zn-MOF-74, the values of the constant n are lower than 1 in both the linear and non-linear fitting and this is an indication that the adsorption is cooperative[90]. The maximum monolayer adsorption capacity was obtained by the RT-Zn_MOF-74 (487 mg/g). This is the highest adsorption capacity ever reported in the literature for the adsorption of lead ions from water after comparing it to many other adsorbents [91-94]. In addition, the monolayer adsorption capacity of the HT-Zn-MOF-74 is 333 mg/g which is also a very high number compared to hundreds of adsorbents reported in the literature. The difference in the performance between the HT and RT Zn-MOF-74 is because of the presence of more active sites in the RT adsorbent than the HT one. The main problem with the HT-Zn_MOF-74 is the agglomeration of the adsorbent micro particles leading

to lower exposure onto the active sites and definitely lower removal efficiency. While in the case of RT-Zn_MOF-74, the dispersion of the nano-particles leads to higher surface exposure and hence the adsorbate would have better chance to interact with the active sites. Similar conclusion was reached when Zn-MOF-74 was used as an adsorbent for removing arsenic As(V) from water[95]. The Dubinin-Radushkevich isotherm model is generally used to represent the adsorption mechanism with a Gaussian energy distribution onto heterogeneous surfaces[96] and to express the adsorption process onto both homogeneous and heterogeneous surfaces[97]. Figure 12 (C) represents the data fitted using D-R model for both HT and RT Zn-MOF-74 with R^2 0.956 and 0.995 respectively. The mean adsorption energy for both adsorbents was found to be less than 8 KJ mol⁻¹ (1 KJ mol⁻¹ for the RT-Zn-MOF-74 and 0.235 KJ mol⁻¹ for the HT-Zn-MOF-74). Therefore physical adsorption is the dominant mechanism in the process of removing lead Pb²⁺ from water and Vander walls forces are the main forces controlling the interaction between the positive sorbate particles and the negative sorbent surface. Adsorption experiments were also conducted on solutions containing ultra-low concentrations of lead ions. The highest removal efficiency attained is 81% (81 µg g⁻¹) when the initial lead concentration in the solution was 100 µg L⁻¹ (Figure 10) . This high uptake at the very low concentration levels reveals a very promising future for the RT-Zn-MOF-74 in industrial usages especially that the threshold concentration of lead ions in drinking water is 15 µg L⁻¹[98].

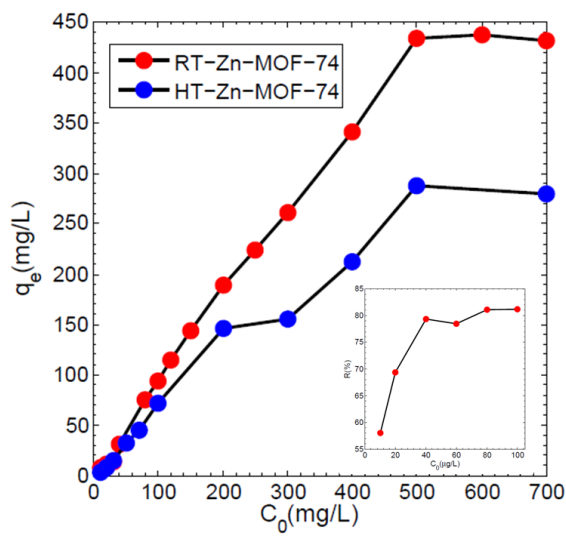


Figure 11: Effect of changing initial lead concentration on the adsorption capacity of RT-Zn-MOF-74.

F. Adsorption Kinetics

To analyze the adsorption mechanism of Pb(II) ions onto RT-Zn-MOF-74, the pseudo first, second order models are used. The pseudo first-order[99] (Eq. 9) and pseudo second-order[100] (Eq. 10) model equations are given as follow:

$$\ln(q_e - q_t) = \ln q_e - k_1 t \quad (9)$$

$$\frac{t}{q_t} = \frac{1}{k_2 q_e^2} + \frac{t}{q_e} \quad (10)$$

where q_e (mg g⁻¹) is equilibrium capacity calculated experimentally, q_t (mg g⁻¹) is the adsorption amount at time t , k_1 (min⁻¹) is the pseudo-first-order rate constant and k_2 (g mmol⁻¹ min⁻¹) is the pseudo second-order rate constant. The results of the kinetic adsorption studies are shown in Figure 11. The kinetic parameters are given in Table 6.

Table 6: parameters of Pb(II) adsorption kinetics by Zn-MOF-74.

Kinetic Model	Parameter	Value
Pseudo-First-Order	q_e (g.mg ⁻¹)	9.54
	k_1 (min ⁻¹)	0.0441
	R^2	0.985
Pseudo-Second-Order	q_e (g.mg ⁻¹)	93.5
	k_2 (g.mg ⁻¹ .min ⁻¹)	0.0346
	R^2	0.999

A pseudo first-order kinetic model, assumes that the rate of change in the solute concentration with time is logarithmically proportional to changes in the saturation concentration and the amount of adsorbent over time[71]. On the other hand, a pseudo second-order kinetic model assumes that the adsorption capacity is proportional to the number of active sites occupied on the adsorbent. Both Pseudo first order and second order models fitted the data with R^2 equals 0.985 and 0.9998 respectively. Due to higher R^2 value of the pseudo second-order model, it is assumed that this model is more favorable in this situation. Having said that, the pseudo second order model reveals a chemical adsorption status and hence it assumes that there is a single monolayer where adsorption is taking place and this is validated in the adsorption isotherm section where Langmuir model also was able to fit the data very well. On the other hand, Dubinin Radushkevich model has fitted the data very well also and from this model we were able to calculate the heat of adsorption. Because the heat of adsorption E (KJ/mol) is found to be 1 KJ/mol which is less than 8 KJ/mol, then it assumes that there is a physical adsorption taking place. By physical adsorption, the molecules are adsorbed forming multiple layers. In this specific experiment, both physisorption and chemisorption are taking place on the surface of the RT-Zn-MOF-74. It might be that a layer of molecules is physically adsorbed on top of an underlying chemisorbed layer[101]. Similar results were obtained by Liping Cheng in the paper “Removal of Pb(II) ions using modified walnut shell”[86].

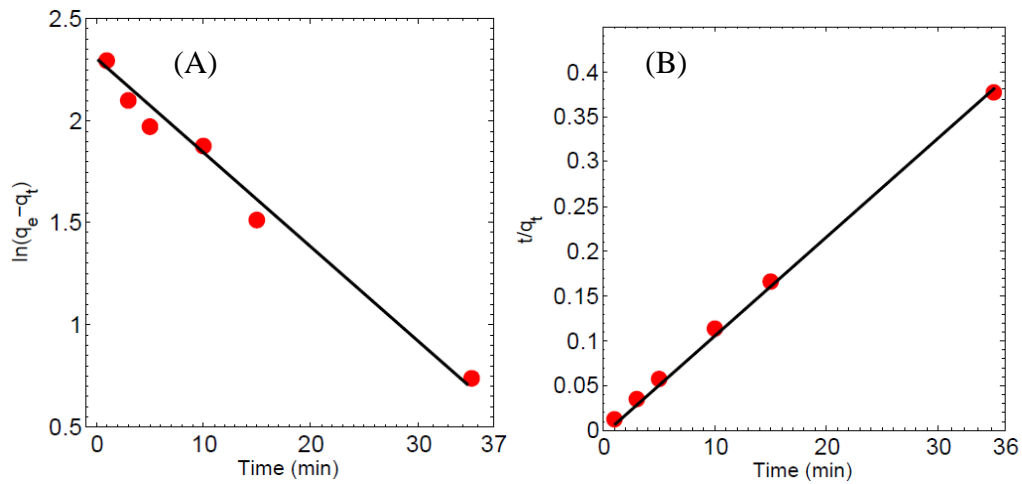


Figure 12: Pseudo first-order kinetics of Pb(II) removal by Zn-MOF-74 (A). Pseudo second-order kinetics of Pb(II) removal by Zn-MOF-74 (B).

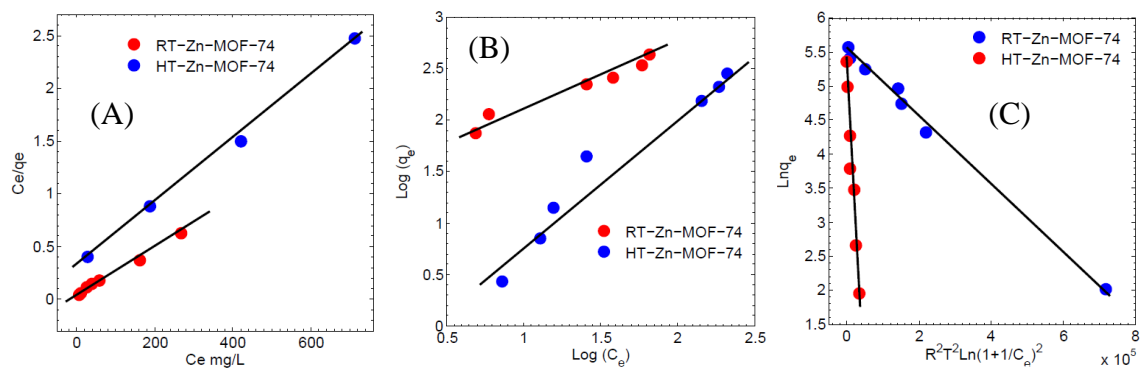


Figure 13: Langmuir isotherm for Pb(II) adsorption onto RT-Zn-MOF-74 and HT-Zn-MOF-74 (A). Freundlich isotherm for Pb(II) adsorption onto RT-Zn-MOF-74 and HT-60

Zn-MOF-74 (B). D-R isotherm for Pb(II) adsorption onto RT-Zn-MOF-74 and HT-Zn-MOF-74 (C).

G. Effect of adsorbent dosage

Figure 13 shows the effect of adsorbent dose on the adsorption capacity of the RT-Zn-MOF-74. The increase in the mass dosage of adsorbent from 2 mg to 20 mg resulted in a decrease in equilibrium adsorption capacity, q_e , of the adsorbent from 335.5 mg g⁻¹ to 46.615 mg g⁻¹ respectively. On the other side, the removal efficiency has increased with the increase of the adsorbent mass added. A similar trend has been reported in different studies [88, 102, 103] in the adsorption of Pb (II) by palm kernel fiber and in the adsorption of Ni (II) on kaolinite clay. The increase in the removal efficiency when increasing the adsorbent dosage might be due to the increase in the surface negativity and decrease in the electrostatic potential close to the surface of the adsorbent that in principle favors the solute-sorbent interaction[104].

However, the adsorption capacity at equilibrium, q_e , of the RT-Zn-MOF-74 has decreased when the dosage increased and this can be attributed to two reasons. The total surface area of the adsorbent decreased and the diffusion path length increased leading to a decrease in the adsorption capacity[105].

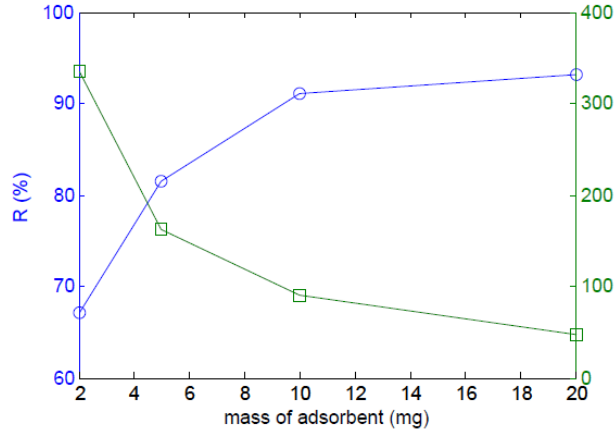


Figure 14: Effect of adsorbent mass dosage on removal efficiency of Pb(II) ions and adsorption capacity of RT-Zn-MOF-74.

H. Thermodynamics

In order to provide information about the thermodynamic feasibility of removing Pb(II) ions from water using RT-Zn-MOF-74, thermodynamic parameters such as enthalpy ΔH^0 , entropy ΔS^0 , and Gibbs free energy ΔG^0 are calculated. The following equations are used to calculate the above mentioned thermodynamic parameters:

$$\ln(K) = -\left(\frac{\Delta H^0}{R}\right)\frac{1}{T} + \frac{\Delta S^0}{R} \quad (11)$$

$$\Delta G^0 = \Delta H^0 - T\Delta S^0 \quad (12)$$

Where K is the equilibrium constant equivalent to q_e/C_e ($L g^{-1}$), T is the operating temperature (K), and R is the gas constant. Equation 12 is the van't hof equation at which the enthalpy can be found from the slope of the plot and the entropy can be found from the y-intercept. Five different runs at five different temperatures (25°C, 30°C, 35°C, 40°C, 50°C) were conducted and the results are shown below in table 7.

Table 7: Thermodynamic properties at T= 25°C, 30°C, 35°C, 40°C, 50°C.

ΔH^0 (KJ mol ⁻¹)	ΔS^0 (J mol ⁻¹ K ⁻¹)	ΔG^0 (KJ mol ⁻¹)				
		298 K	303 K	308 K	313 K	323 K
20.9	92.2	-6.51	-6.96	-7.43	-7.88	-8.81

The negative value of ΔG^0 indicates that the adsorption of Pb(II) ions onto the surface of RT-Zn-MOF-74 is spontaneous. As the temperature increases, the ΔG^0 value becomes more negative suggesting that high temperatures are more favorable for the removal of Pb(II) ions. The enthalpy of the process was found to be 20.9 KJ mol⁻¹ which means that the adsorption is endothermic. Because the calculated value of enthalpy is less than 40 KJ mol⁻¹, then this is another added evidence that the process is more of physical

adsorption than chemical adsorption. Finally, the positive value of the entropy indicates that the process of removing lead ions by RT-Zn-MOF-74 is entropy driven.

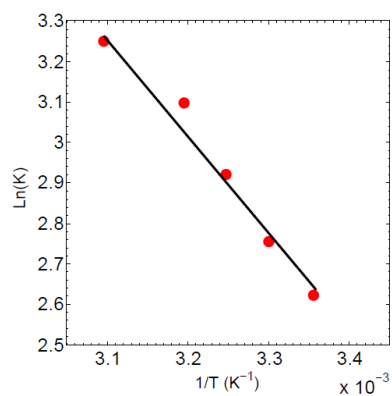


Figure 15: Van't Hof plot of $\ln(K)$ versus inverse temperature for $T = 25\text{ }^{\circ}\text{C}$, $30\text{ }^{\circ}\text{C}$, $35\text{ }^{\circ}\text{C}$, $40\text{ }^{\circ}\text{C}$ and $50\text{ }^{\circ}\text{C}$.

CHAPTER VII

CONCLUSION

In this study, Zn-MOF-74 was investigated for the first time as sorbent for arsenic and lead removal from water. The effect of particle size on the adsorption properties was evaluated by studying two sets of MOF-74 samples synthesized in a two-size regime (nano and microsized). Interestingly, the nano-sized MOF removed two time more As(V) and Pb(II) from water than the conventional MOF-74 (99.0 mg g^{-1} vs 48.7 mg g^{-1}) and (487 mg g^{-1} vs 379 mg g^{-1}) respectively. This can be explained by the creation of more adsorption sites and less agglomeration at the nanoscale, which enhance the As(V) and Pb(II) removal efficiency. Furthermore, the thermodynamic and kinetic parameters were investigated and showed that the adsorption of As(V) on the MOF nanocrystals was an endothermic process and chemisorption processes were evidenced while for the adsorption of Pb(II) the process was endothermic and physical adsorption was noticed. These results were also demonstrated using two other modules (intra-particle diffusion) and (Dubinin–Radushkevich). Finally, this work demonstrated the importance of size tuning of the adsorbent and gave a promising assessment for possible application of nano-Zn-MOF-74 in industrial waste water treatment for removing As(V) and Pb(II) especially after showing extremely high uptake at the ultra-low concentration levels.

APPENDIX I

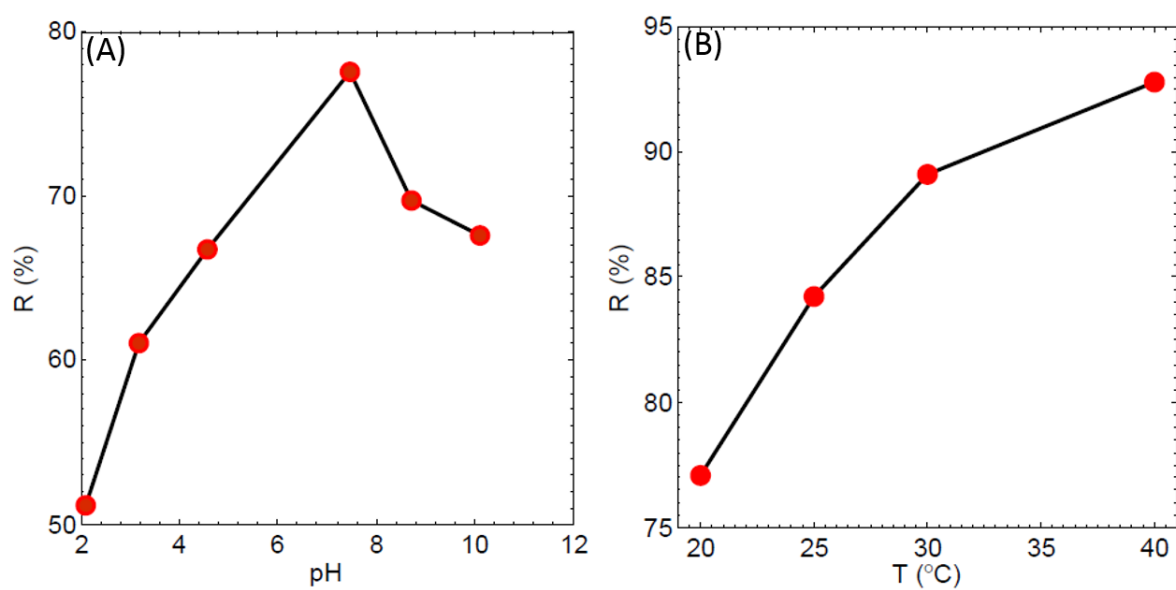


Figure S1. Effects of pH on the percent removal of As(V), by the adsorbent Zn-MOF-74. $C_0 = 40 \text{ mg L}^{-1}$, $V = 10 \text{ mL}$, $m = 10 \text{ mg}$, $t = 1 \text{ hr}$ (A). Effects of Temperature on the

As(V) removal by the adsorbent Zn-MOF-74. $C_0 = 40 \text{ mg L}^{-1}$, $V = 10 \text{ mL}$, $m = 10 \text{ mg}$, $t = 1 \text{ hr}$ (B).

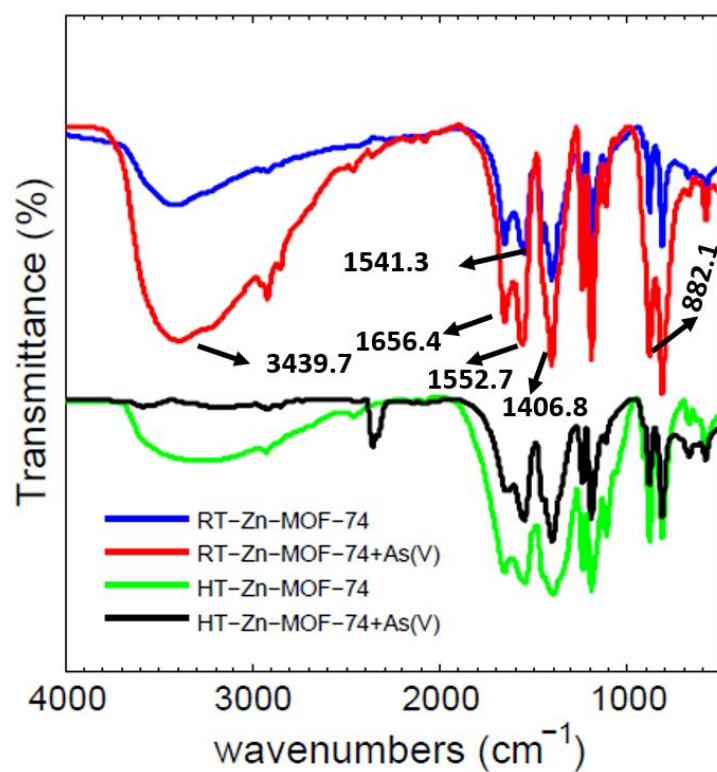


Figure S2. FT-IR spectra of RT and HT-Zn-MOF-74 before and after adsorption of As(V).

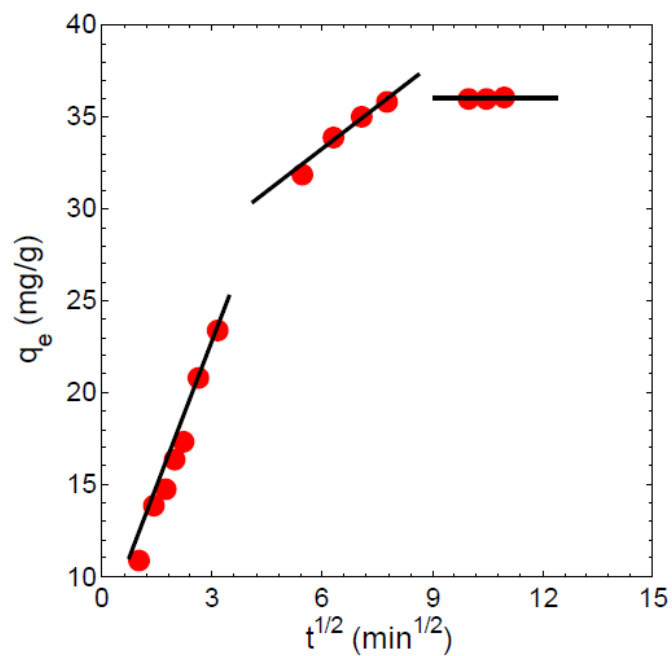


Figure S3. Intraparticle diffusion kinetics of As(V) on RT-Zn-MOF-74 nanoparticles.

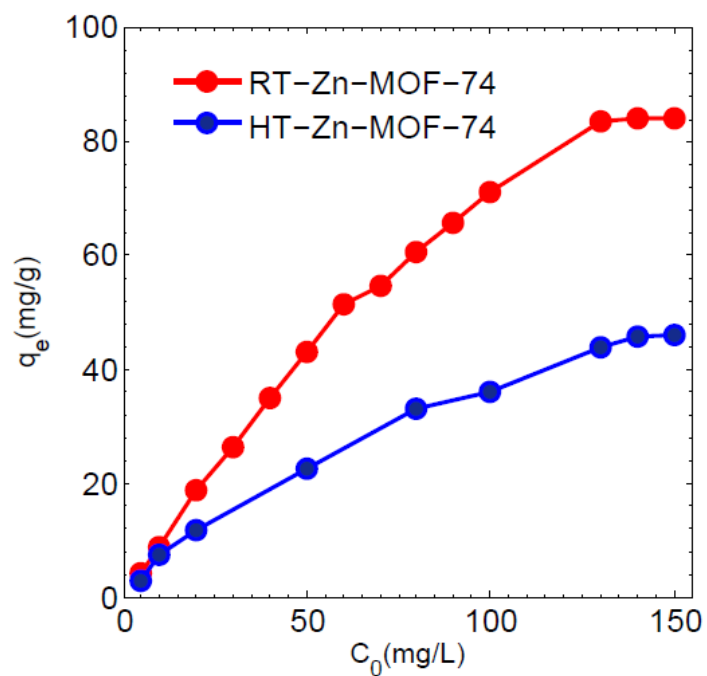


Figure S4. Effect of initial concentration of As(V) on the adsorption onto RT-Zn-MOF-74 and HT-Zn-MOF-74. $T = 25\text{ }^\circ\text{C}$, $V = 10\text{ mL}$, $\text{pH} = 7.8$, $m = 10\text{ mg}$.

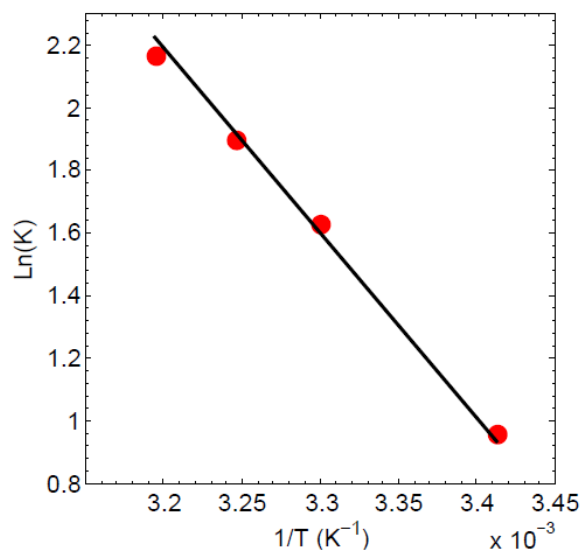


Figure S5. Van't Hof plot of $\ln(K)$ versus inverse temperature ($R^2 = 0.998$) for $T = 20$ °C, 30 °C, 35 °C and 40 °C.

Tables S1 and S2 below represents a sample calculation for finding the isotherm parameters mentioned in the thesis above.

Table S1: Sample calculation for isotherm models parameters in the adsorption of Arsenic As(V).

C _o (mg/L)	C _e (mg/L)	Adsorbent Mass (g)	V (L)	q _e (mg g ⁻¹)	1/q _e	1/C _e	logq _e	logC _e	c _e /q _e
5	0.81	0.01	0.01	4.19	0.238	1.23	0.62	-0.0915	0.19
10	1.13	0.01	0.01	8.87	0.11	0.88	0.94	0.05307	0.127
20	1.27	0.01	0.01	18.73	0.053	0.787	1.27	0.103	0.067
30	3.54	0.01	0.01	26.46	0.0377	0.282	1.42	0.549	0.133
40	4.91	0.01	0.01	35.09	0.028	0.203	1.54	0.691	0.139
50	6.81	0.01	0.01	43.19	0.0231	0.146	1.63	0.833	0.157
60	8.44	0.01	0.01	51.56	0.0193	0.118	1.71	0.926	0.163
70	15.4	0.01	0.01	54.6	0.0183	0.064	1.73	1.187	0.282
80	19.32	0.01	0.01	60.68	0.016	0.051	1.78	1.28	0.318
90	24.244	0.01	0.01	65.756	0.0152	0.041	1.81	1.38	0.368
100	28.84	0.01	0.01	71.16	0.0140	0.034	1.85	1.45	0.405
110	42.69	0.01	0.01	67.31	0.0148	0.023	1.82	1.63	0.63
120	44.82	0.01	0.01	75.18	0.0133	0.022	1.87	1.65	0.596
130	46.4	0.01	0.01	83.6	0.0119	0.021	1.92	1.66	0.555
140	55.8	0.01	0.01	84.2	0.0118	0.017	1.92	1.74	0.662
150	51.76	0.01	0.01	98.24	0.010	0.019	1.99	1.71	0.526

Table S2: Sample calculation for isotherm models parameters in the adsorption of lead.

C _o (ppm)	C _e (ppm)	R (%)	q _e (mg/g)	c _e /q _e	logC _e	logq _e	R*T	ln(1+(1/C _e))	epsil ²	lnq _e
10	7.3	27	2.7	2.7	0.86	0.431	2519	0.128	104594.3	0.993
20	12.94	35.3	7.06	1.83	1.11	0.848	2519	0.0744	35164.76	1.95
30	15.79	47.3	14.21	1.11	1.19	1.15	2519	0.0614	23929.63	2.65
50	17.644	64.7	32.356	0.545	1.24	1.51	2519	0.0551	19286.76	3.47
70	25.63	63.3	44.37	0.577	1.40	1.64	2519	0.0382	9296.779	3.792
100	28.67	71.3	71.33	0.401	1.45	1.85	2519	0.0342	7459.634	4.26
200	53.51	73.2	146.49	0.36	1.72	2.16	2519	0.0185	2175.614	4.98
300	144.35	51.8	155.65	0.92	2.15	2.19	2519	0.0069	302.4626	5.04
400	187.66	53.1	212.34	0.88	2.27	2.32	2519	0.00531	179.2473	5.35
500	212.5	57.5	287.5	0.739	2.32	2.45	2519	0.00469	139.8774	5.66
700	420	40	280	1.5	2.62	2.44	2519	0.00237	35.89002	5.63
1000	712.3	28.7	287.7	2.47	2.85	2.45	2519	0.0014	12.49022	5.66

BIBLIOGRAPHY

- [1] Y. Sun, G. Zhou, X. Xiong, X. Guan, L. Li, H. Bao, Enhanced arsenite removal from water by Ti (SO₄)₂ coagulation, *Water Research* 47 (2013) 4340-4348.
- [2] B.V. Tangahu, S.R. Sheikh Abdullah, H. Basri, M. Idris, N. Anuar, M. Mukhlisin, A Review on heavy metals (As, Pb, and Hg) uptake by plants through phytoremediation, *International Journal of Chemical Engineering* 2011 (2011).
- [3] P. Drahota, M. Filippi, Secondary arsenic minerals in the environment: a review, *Environment International* 35 (2009) 1243-1255.
- [4] P. Riveros, J. Dutrizac, P. Spencer, Arsenic disposal practices in the metallurgical industry, *Canadian Metallurgical Quarterly* 40 (2001) 395-420.
- [5] B. Manna, U.C. Ghosh, Adsorption of arsenic from aqueous solution on synthetic hydrous stannic oxide, *Journal of Hazardous Materials* 144 (2007) 522-531.
- [6] D. Mohan, C.U. Pittman, Arsenic removal from water/wastewater using adsorbents—a critical review, *Journal of Hazardous Materials* 142 (2007) 1-53.
- [7] U. Epa, National Primary Drinking Water Regulations: Arsenic and Clarifications to Compliance and New Source Contaminants Monitoring, *Federal Register* 66 (2001) 6975-7066.
- [8] R.N. Ratnaïke, Acute and chronic arsenic toxicity, *Postgraduate medical journal* 79 (2003) 391-396.
- [9] C.-J. Chen, Y.-M. Hsueh, M.-S. Lai, M.-P. Shyu, S.-Y. Chen, M.-M. Wu, T.-L. Kuo, T.-Y. Tai, Increased prevalence of hypertension and long-term arsenic exposure, *Hypertension* 25 (1995) 53-60.
- [10] M.R. Karagas, T.A. Stukel, T.D. Tosteson, Assessment of cancer risk and environmental levels of arsenic in New Hampshire, *International journal of hygiene and environmental health* 205 (2002) 85-94.
- [11] J.-T. Dong, X.-M. Luo, Effects of arsenic on DNA damage and repair in human fetal lung fibroblasts, *Mutation Research/DNA Repair* 315 (1994) 11-15.
- [12] J.C. Ng, J. Wang, A. Shraim, A global health problem caused by arsenic from natural sources, *Chemosphere* 52 (2003) 1353-1359.
- [13] P.B. Tchounwou, C.G. Yedjou, A.K. Patlolla, D.J. Sutton, Heavy metal toxicity and the environment, *Molecular, clinical and environmental toxicology*, Springer 2012, pp. 133-164.
- [14] S. Srikanan, Pectin: Panacea for both lead poisoning and lead contamination.
- [15] F. Cuenot, M. Meyer, A. Bucaille, R. Guillard, A molecular approach to remove lead from drinking water, *Journal of molecular liquids* 118 (2005) 89-99.
- [16] A. Dungca, THE REMOVAL OF LEAD FROM WATER USING IONIC LIQUID, WORCESTER POLYTECHNIC INSTITUTE.

- [17] Y. Tian, B. Gao, V.L. Morales, L. Wu, Y. Wang, R. Muñoz-Carpena, C. Cao, Q. Huang, L. Yang, Methods of using carbon nanotubes as filter media to remove aqueous heavy metals, *Chemical Engineering Journal* 210 (2012) 557-563.
- [18] S. Kumar, R.R. Nair, P.B. Pillai, S.N. Gupta, M. Iyengar, A. Sood, Graphene oxide–MnFe₂O₄ magnetic nanohybrids for efficient removal of lead and arsenic from water, *ACS applied materials & interfaces* 6 (2014) 17426-17436.
- [19] P. Visoottiviseth, K. Francesconi, W. Sridokchan, The potential of Thai indigenous plant species for the phytoremediation of arsenic contaminated land, *Environmental pollution* 118 (2002) 453-461.
- [20] I. Alkorta, J. Hernández-Allica, C. Garbisu, Plants against the global epidemic of arsenic poisoning, *Environment international* 30 (2004) 949-951.
- [21] F.E. Chigbo, R.W. Smith, F.L. Shore, Uptake of arsenic, cadmium, lead and mercury from polluted waters by the water hyacinth *Eichornia crassipes*, *Environmental Pollution Series A, Ecological and Biological* 27 (1982) 31-36.
- [22] H. Cui, Y. Su, Q. Li, S. Gao, J.K. Shang, Exceptional arsenic (III, V) removal performance of highly porous, nanostructured ZrO₂ spheres for fixed bed reactors and the full-scale system modeling, *Water research* 47 (2013) 6258-6268.
- [23] T.-F. Lin, J.-K. Wu, Adsorption of arsenite and arsenate within activated alumina grains: equilibrium and kinetics, *Water research* 35 (2001) 2049-2057.
- [24] B. Arstad, H. Fjellvåg, K.O. Kongshaug, O. Swang, R. Blom, Amine functionalised metal organic frameworks (MOFs) as adsorbents for carbon dioxide, *Adsorption* 14 (2008) 755-762.
- [25] C. Janiak, J.K. Vieth, MOFs, MILs and more: concepts, properties and applications for porous coordination networks (PCNs), *New Journal of Chemistry* 34 (2010) 2366-2388.
- [26] J.L. Rowsell, O.M. Yaghi, Metal–organic frameworks: a new class of porous materials, *Microporous and Mesoporous Materials* 73 (2004) 3-14.
- [27] M.C. Das, S. Xiang, Z. Zhang, B. Chen, Functional mixed metal–organic frameworks with metalloligands, *Angewandte Chemie International Edition* 50 (2011) 10510-10520.
- [28] O.M. Yaghi, M. O'keeffe, N.W. Ockwig, H.K. Chae, M. Eddaoudi, J. Kim, Reticular synthesis and the design of new materials, *Nature* 423 (2003) 705-714.
- [29] F. Luo, J.L. Chen, L.L. Dang, W.N. Zhou, H.L. Lin, J.Q. Li, S.J. Liu, M.B. Luo, High-performance Hg²⁺ removal from ultra-low-concentration aqueous solution using both acylamide- and hydroxyl-functionalized metal–organic framework, *Journal of Materials Chemistry A* 3 (2015) 9616-9620.
- [30] S. Zuluaga, E.M. Fuentes-Fernandez, K. Tan, F. Xu, J. Li, Y.J. Chabal, T. Thonhauser, Understanding and controlling water stability of MOF-74, *Journal of Materials Chemistry A* 4 (2016) 5176-5183.

- [31] J.J. Pignatello, E. Oliveros, A. MacKay, Advanced oxidation processes for organic contaminant destruction based on the Fenton reaction and related chemistry, *Critical reviews in environmental science and technology* 36 (2006) 1-84.
- [32] Y. Ku, I.-L. Jung, Photocatalytic reduction of Cr (VI) in aqueous solutions by UV irradiation with the presence of titanium dioxide, *Water Research* 35 (2001) 135-142.
- [33] M. Karnib, A. Kabbani, H. Holail, Z. Olama, Heavy metals removal using activated carbon, silica and silica activated carbon composite, *Energy Procedia* 50 (2014) 113-120.
- [34] E. López-Maldonado, M. Oropeza-Guzman, J. Jurado-Baizaval, A. Ochoa-Terán, Coagulation–flocculation mechanisms in wastewater treatment plants through zeta potential measurements, *Journal of hazardous materials* 279 (2014) 1-10.
- [35] S.-H. Lin, R.-S. Juang, Heavy metal removal from water by sorption using surfactant-modified montmorillonite, *Journal of Hazardous Materials* 92 (2002) 315-326.
- [36] M. Komárek, A. Vaněk, V. Ettler, Chemical stabilization of metals and arsenic in contaminated soils using oxides—a review, *Environmental Pollution* 172 (2013) 9-22.
- [37] N. Dizge, B. Keskinler, H. Barlas, Sorption of Ni (II) ions from aqueous solution by Lewatit cation-exchange resin, *Journal of hazardous materials* 167 (2009) 915-926.
- [38] S. Gunatilake, Methods of removing heavy metals from industrial wastewater, *Methods* 1 (2015).
- [39] D. Lakherwal, Adsorption of heavy metals: a review, *International journal of environmental research and development* 4 (2014) 41-48.
- [40] W.C. Leung, M.-F. Wong, H. Chua, W. Lo, P. Yu, C. Leung, Removal and recovery of heavy metals by bacteria isolated from activated sludge treating industrial effluents and municipal wastewater, *Water science and technology* 41 (2000) 233-240.
- [41] T.A. Kurniawan, G.Y. Chan, W.-h. Lo, S. Babel, Comparisons of low-cost adsorbents for treating wastewaters laden with heavy metals, *Science of the total environment* 366 (2006) 409-426.
- [42] J.-H. Huang, A. Voegelin, S.A. Pombo, A. Lazzaro, J. Zeyer, R. Kretzschmar, Influence of arsenate adsorption to ferrihydrite, goethite, and boehmite on the kinetics of arsenate reduction by *Shewanella putrefaciens* strain CN-32, *Environmental science & technology* 45 (2011) 7701-7709.
- [43] H. Zhu, Y. Jia, X. Wu, H. Wang, Removal of arsenic from water by supported nano zero-valent iron on activated carbon, *Journal of Hazardous Materials* 172 (2009) 1591-1596.
- [44] J. Rivera-Utrilla, I. Bautista-Toledo, M.A. Ferro-García, C. Moreno-Castilla, Activated carbon surface modifications by adsorption of bacteria and their effect on aqueous lead adsorption, *Journal of Chemical Technology and biotechnology* 76 (2001) 1209-1215.

- [45] L. Zeng, Arsenic adsorption from aqueous solutions on an Fe (III)-Si binary oxide adsorbent, *Water Quality Research Journal of Canada* 39 (2004) 267-275.
- [46] C. Wang, X. Liu, J.P. Chen, K. Li, Superior removal of arsenic from water with zirconium metal-organic framework UiO-66, *Scientific reports* 5 (2015) 16613.
- [47] T. Tuutijärvi, J. Lu, M. Sillanpää, G. Chen, As (V) adsorption on maghemite nanoparticles, *Journal of Hazardous Materials* 166 (2009) 1415-1420.
- [48] C.-S. Jeon, K. Baek, J.-K. Park, Y.-K. Oh, S.-D. Lee, Adsorption characteristics of As (V) on iron-coated zeolite, *Journal of Hazardous Materials* 163 (2009) 804-808.
- [49] M. Mouflih, A. Aklil, S. Sebti, Removal of lead from aqueous solutions by activated phosphate, *Journal of Hazardous Materials* 119 (2005) 183-188.
- [50] I.W. Nah, K.-Y. Hwang, C. Jeon, H.B. Choi, Removal of Pb ion from water by magnetically modified zeolite, *Minerals Engineering* 19 (2006) 1452-1455.
- [51] V.K. Gupta, A. Rastogi, Biosorption of lead (II) from aqueous solutions by non-living algal biomass *Oedogonium* sp. and *Nostoc* sp.—a comparative study, *Colloids and Surfaces B: Biointerfaces* 64 (2008) 170-178.
- [52] X. Luo, C. Wang, S. Luo, R. Dong, X. Tu, G. Zeng, Adsorption of As (III) and As (V) from water using magnetite Fe₃O₄-reduced graphite oxide–MnO₂ nanocomposites, *Chemical Engineering Journal* 187 (2012) 45-52.
- [53] B. Pan, Q. Zhang, W. Zhang, B. Pan, W. Du, L. Lv, Q. Zhang, Z. Xu, Q. Zhang, Highly effective removal of heavy metals by polymer-based zirconium phosphate: a case study of lead ion, *Journal of colloid and interface science* 310 (2007) 99-105.
- [54] D. Feng, C. Aldrich, Adsorption of heavy metals by biomaterials derived from the marine alga *Ecklonia maxima*, *Hydrometallurgy* 73 (2004) 1-10.
- [55] H.-C. Zhou, J.R. Long, O.M. Yaghi, *Introduction to metal–organic frameworks*, ACS Publications, 2012.
- [56] T.G. Glover, G.W. Peterson, B.J. Schindler, D. Britt, O. Yaghi, MOF-74 building unit has a direct impact on toxic gas adsorption, *Chemical Engineering Science* 66 (2011) 163-170.
- [57] H.-Y. Cho, D.-A. Yang, J. Kim, S.-Y. Jeong, W.-S. Ahn, CO₂ adsorption and catalytic application of Co-MOF-74 synthesized by microwave heating, *Catalysis today* 185 (2012) 35-40.
- [58] D.-A. Yang, H.-Y. Cho, J. Kim, S.-T. Yang, W.-S. Ahn, CO₂ capture and conversion using Mg-MOF-74 prepared by a sonochemical method, *Energy & Environmental Science* 5 (2012) 6465-6473.
- [59] P. Verma, X. Xu, D.G. Truhlar, Adsorption on Fe-MOF-74 for C₁–C₃ hydrocarbon separation, *The Journal of Physical Chemistry C* 117 (2013) 12648-12660.
- [60] Y.Y. Xiong, J.Q. Li, L. Le Gong, X.F. Feng, L.N. Meng, L. Zhang, P.P. Meng, M.B. Luo, F. Luo, Using MOF-74 for Hg²⁺ removal from ultra-low concentration aqueous solution, *Journal of Solid State Chemistry* 246 (2017) 16-22.

- [61] P.D. Dietzel, R.E. Johnsen, R. Blom, H. Fjellvåg, Structural changes and coordinatively unsaturated metal atoms on dehydration of honeycomb analogous microporous metal–organic frameworks, *Chem. Eur. J.* 14 (2008) 2389-2397.
- [62] P.D. Dietzel, R. Blom, H. Fjellvåg, Base-Induced Formation of Two Magnesium Metal-Organic Framework Compounds with a Bifunctional Tetratopic Ligand, *Eur. J. Inorg. Chem.* 2008 (2008) 3624-3632.
- [63] L.J. Wang, H. Deng, H. Furukawa, F. Gándara, K.E. Cordova, D. Peri, O.M. Yaghi, Synthesis and characterization of metal–organic framework-74 containing 2, 4, 6, 8, and 10 different metals, *Inorg. Chem.* 53 (2014) 5881-5883.
- [64] M. Díaz-García, Á. Mayoral, I. Díaz, M. Sánchez-Sánchez, Nanoscaled M-MOF-74 Materials Prepared at Room Temperature, *Cryst. Growth Des.* 14 (2014) 2479-2487.
- [65] D.-A. Yang, H.-Y. Cho, J. Kim, S.-T. Yang, W.-S. Ahn, CO₂ capture and conversion using Mg-MOF-74 prepared by a sonochemical method, *EES* 5 (2012) 6465-6473.
- [66] B. Heibati, M. Ghoochani, A.B. Albadarin, A. Mesdaghinia, A.S.H. Makhlof, M. Asif, A. Maity, I. Tyagi, S. Agarwal, V.K. Gupta, Removal of linear alkyl benzene sulfonate from aqueous solutions by functionalized multi-walled carbon nanotubes, *J. Mol. Liq.* 213 (2016) 339-344.
- [67] M. Lim, G.-C. Han, J.-W. Ahn, K.-S. You, H.-S. Kim, Leachability of arsenic and heavy metals from mine tailings of abandoned metal mines, *Int. J. Environ. Res. Public Health* 6 (2009) 2865-2879.
- [68] M. Grafe, M.J. Eick, P.R. Grossl, A.M. Saunders, Adsorption of arsenate and arsenite on ferrihydrite in the presence and absence of dissolved organic carbon, *J. Environ. Qual.* 31 (2002) 1115-1123.
- [69] M. Jian, B. Liu, G. Zhang, R. Liu, X. Zhang, Adsorptive removal of arsenic from aqueous solution by zeolitic imidazolate framework-8 (ZIF-8) nanoparticles, *Colloids Surf., A* 465 (2015) 67-76.
- [70] B.J. Abu Tarboush, M.M. Husein, Oxidation of asphaltenes adsorbed onto NiO nanoparticles, *Appl. Catal., A* 445-446 (2012) 166-171.
- [71] M. Kitis, E. Karakaya, N.O. Yigit, G. Civelekoglu, A. Akcil, Heterogeneous catalytic degradation of cyanide using copper-impregnated pumice and hydrogen peroxide, *Water Research* 39 (2005) 1652-1662.
- [72] L. Li, W. Ma, S. Shen, H. Huang, Y. Bai, H. Liu, A Combined Experimental and Theoretical Study on the Extraction of Uranium by Amino-Derived Metal-Organic Frameworks through Post-Synthetic Strategy, *ACS Appl. Mater. Interfaces* 8 (2016) 31032-31041.
- [73] V. Srihari, A. Das, The kinetic and thermodynamic studies of phenol-sorption onto three agro-based carbons, *Desalination* 225 (2008) 220-234.

- [74] N. Kannan, M.M. Sundaram, Kinetics and mechanism of removal of methylene blue by adsorption on various carbons—a comparative study, *Dyes Pigm.* 51 (2001) 25-40.
- [75] K.V. Kumar, K. Porkodi, Mass transfer, kinetics and equilibrium studies for the biosorption of methylene blue using *Paspalum notatum*, *J. Hazard. Mater.* 146 (2007) 214-226.
- [76] A. Goswami, P. Raul, M. Purkait, Arsenic adsorption using copper (II) oxide nanoparticles, *Chem. Eng. Res. Des.* 90 (2012) 1387-1396.
- [77] T.M. Suzuki, J.O. Bomani, H. Matsunaga, T. Yokoyama, Preparation of porous resin loaded with crystalline hydrous zirconium oxide and its application to the removal of arsenic, *React. Funct. Polym.* 43 (2000) 165-172.
- [78] H. Matsunaga, T. Yokoyama, R.J. Eldridge, B.A. Bolto, Adsorption characteristics of arsenic (III) and arsenic (V) on iron (III)-loaded chelating resin having lysine-N α , N α -diacetic acid moiety, *React. Funct. Polym.* 29 (1996) 167-174.
- [79] F.-S. Zhang, H. Itoh, Iron oxide-loaded slag for arsenic removal from aqueous system, *Chemosphere* 60 (2005) 319-325.
- [80] S. Bang, X. Meng, G.P. Korfiatis, Removal of arsenic from water by zero-valent iron, *J. Hazard. Mater.* 121 (2002) 61-67.
- [81] G.E. Fryxell, J. Liu, T.A. Hauser, Z. Nie, K.F. Ferris, S. Mattigod, M. Gong, R.T. Hallen, Design and synthesis of selective mesoporous anion traps, *Chem. Mater.* 11 (1999) 2148-2154.
- [82] B.J. Abu Tarboush, M.M. Husein, Inferring the role of NiO nanoparticles from the thermal behavior of virgin and adsorbed hydrocarbons, *Fuel* 147 (2015) 53-61.
- [83] M. Sekar, V. Sakthi, S. Rengaraj, Kinetics and equilibrium adsorption study of lead (II) onto activated carbon prepared from coconut shell, *J. Colloid Interface Sci.* 279 (2004) 307-313.
- [84] Y. Li, X. Wang, D. Xu, J.D. Chung, M. Kaviani, B. Huang, H₂O Adsorption/Desorption in MOF-74: Ab Initio Molecular Dynamics and Experiments, *J. Phys. Chem. C* 119 (2015) 13021-13031.
- [85] O.A. Yeshchenko, I.M. Dmitruk, A.A. Alexeenko, A.V. Kotko, J. Verdal, A.O. Pinchuk, Size and temperature effects on the surface plasmon resonance in silver nanoparticles, *Plasmonics* 7 (2012) 685-694.
- [86] L. Cheng, L. Sun, W. Xue, Z. Zeng, S. Li, Adsorption equilibrium and kinetics of Pb (II) from aqueous solution by modified walnut shell, *Environmental Progress & Sustainable Energy* 35 (2016) 1724-1731.
- [87] A. Farghali, M. Bahgat, A.E. Allah, M. Khedr, Adsorption of Pb (II) ions from aqueous solutions using copper oxide nanostructures, *Beni-Suef University Journal of Basic and Applied Sciences* 2 (2013) 61-71.

- [88] Y.-S. Ho, A.E. Ofomaja, Kinetics and thermodynamics of lead ion sorption on palm kernel fibre from aqueous solution, *Process biochemistry* 40 (2005) 3455-3461.
- [89] S.V. Mohan, J. Karthikeyan, Removal of lignin and tannin colour from aqueous solution by adsorption onto activated charcoal, *Environmental Pollution* 97 (1997) 183-187.
- [90] U. Kumar, M. Bandyopadhyay, Sorption of cadmium from aqueous solution using pretreated rice husk, *Bioresource technology* 97 (2006) 104-109.
- [91] S. Gueu, B. Yao, K. Adouby, G. Ado, Kinetics and thermodynamics study of lead adsorption on to activated carbons from coconut and seed hull of the palm tree, *International Journal of Environmental Science & Technology* 4 (2007) 11-17.
- [92] Y. Ho, G. McKay, The sorption of lead (II) ions on peat, *Water research* 33 (1999) 578-584.
- [93] A. Demirbas, Heavy metal adsorption onto agro-based waste materials: a review, *Journal of hazardous materials* 157 (2008) 220-229.
- [94] F.F. Orumwense, Removal of lead from water by adsorption on a kaolinitic clay, *Journal of Chemical Technology & Biotechnology: International Research in Process, Environmental AND Clean Technology* 65 (1996) 363-369.
- [95] B.J. Abu Tarboush, A. Chouman, A. Jonderian, M. Ahmad, M. Hmadeh, M. Al-Ghoul, Metal Organic Framework-74 for Ultra-Trace Arsenic Removal from Water: Experimental and Density Functional Theory Studies, *ACS Applied Nano Materials* (2018).
- [96] A. Dada, A. Olalekan, A. Olatunya, O. Dada, Langmuir, Freundlich, Temkin and Dubinin–Radushkevich isotherms studies of equilibrium sorption of Zn²⁺ unto phosphoric acid modified rice husk, *IOSR Journal of Applied Chemistry* 3 (2012) 38-45.
- [97] C.C. Nnaji, C.J. Ebeagwu, E.I. Ugwu, Physicochemical conditions for adsorption of lead from water by rice husk ash, *BioResources* 12 (2016) 799-818.
- [98] H. Dapul, D. Laraque, Lead poisoning in children, *Advances in pediatrics* 61 (2014) 313-333.
- [99] Y.Y. Xiong, J.Q. Li, L. Le Gong, X.F. Feng, L.N. Meng, L. Zhang, P.P. Meng, M.B. Luo, F. Luo, Using MOF-74 for Hg²⁺ removal from ultra-low concentration aqueous solution, *Journal of Solid State Chemistry* 246 (2017) 16-22.
- [100] L. Li, W. Ma, S. Shen, H. Huang, Y. Bai, H. Liu, A Combined Experimental and Theoretical Study on the Extraction of Uranium by Amino-Derived Metal-Organic Frameworks through Post-Synthetic Strategy, *ACS Appl. Mater. Interfaces* 8 (2016) 31032-31041.
- [101] P.A. Webb, Introduction to chemical adsorption analytical techniques and their applications to catalysis, Micromeritics Instrument Corp. Technical Publications (2003).

- [102] E. Unuabonah, B. Olu-Owolabi, K. Adebawale, A. Ofomaja, Adsorption of lead and cadmium ions from aqueous solutions by tripolyphosphate-impregnated Kaolinite clay, *Colloids and Surfaces A: Physicochemical and Engineering Aspects* 292 (2007) 202-211.
- [103] S.S. Gupta, K.G. Bhattacharyya, Adsorption of Ni (II) on clays, *Journal of colloid and interface science* 295 (2006) 21-32.
- [104] E. Unuabonah, K. Adebawale, B. Olu-Owolabi, L. Yang, L. Kong, Adsorption of Pb (II) and Cd (II) from aqueous solutions onto sodium tetraborate-modified kaolinite clay: equilibrium and thermodynamic studies, *Hydrometallurgy* 93 (2008) 1-9.
- [105] A. Shukla, Y.-H. Zhang, P. Dubey, J. Margrave, S.S. Shukla, The role of sawdust in the removal of unwanted materials from water, *Journal of Hazardous Materials* 95 (2002) 137-152.

